Cell Reports

Article

14-3-3 proteins stabilize LGI1-ADAM22 levels to regulate seizure thresholds in mice

Graphical abstract

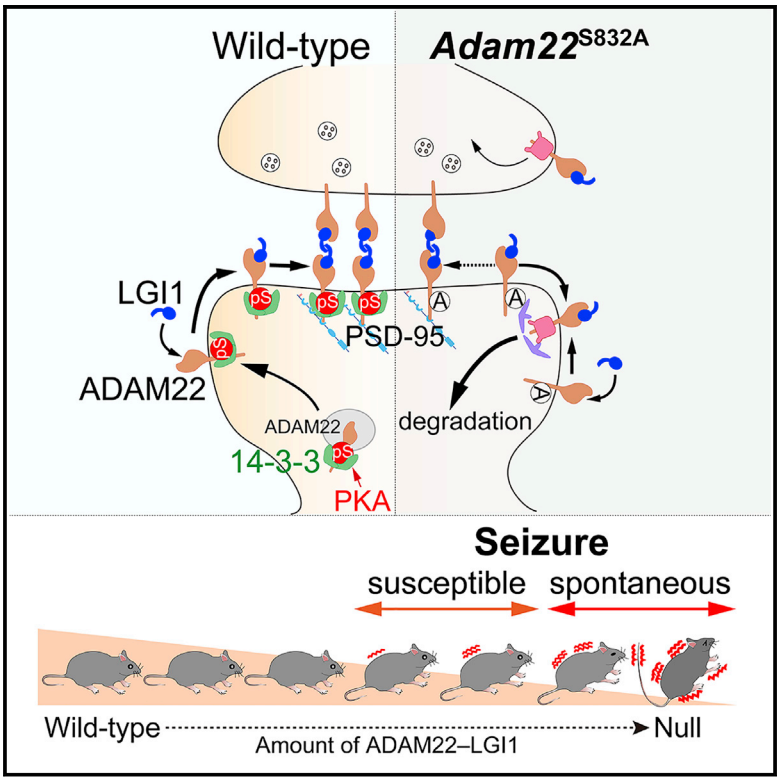

Authors

Norihiko Yokoi, Yuko Fukata, Kei Okatsu, ..., Masumi Hirabayashi, Shuya Fukai, Masaki Fukata

Correspondence

yfukata@nips.ac.jp (Y.F.), mfukata@nips.ac.jp (M.F.)

In brief

Yokoi et al. tackle the question of how much protein function needs to be restored in loss-of-function genetic diseases. Developing hypomorphic mouse models, they estimate minimal levels of a key determinant of epilepsy phenotypes. They propose that biogenesis pathways of the determinant protein could be promising anti-epilepsy drug targets.

Highlights

- Dual phosphorylation of ADAM22 mediates high-affinity binding to dimerized 14-3-3
- Quantitative 14-3-3 interaction protects ADAM22 from endocytosis-mediated degradation
- PKA activation enhances ADAM22-14-3-3 binding to increase ADAM22 protein levels
- Ten percent of ADAM22 residual levels is sufficient to suppress epilepsy in mouse models

Yokoi et al., 2021, Cell Reports 37, 110107
December 14, 2021
https://doi.org/10.1016/j.celrep.2021.110107

Cell Reports

CellPress
OPEN ACCESS

Article

14-3-3 proteins stabilize LGI1-ADAM22 levels to regulate seizure thresholds in mice

Norihiko Yokoi,[1,2] Yuko Fukata,[1,2,*] Kei Okatsu,[3] Atsushi Yamagata,[4] Yan Liu,[3] Makoto Sanbo,[5] Yuri Miyazaki,[1,2] Teppei Goto,[5] Manabu Abe,[6] Hidetoshi Kassai,[7] Kenji Sakimura,[6] Dies Meijer,[8] Masumi Hirabayashi,[2,5] Shuya Fukai,[3] and Masaki Fukata[1,2,9,*]

[1]Division of Membrane Physiology, Department of Molecular and Cellular Physiology, National Institute for Physiological Sciences, National Institutes of Natural Sciences, Okazaki, Aichi 444-8787, Japan
[2]Department of Physiological Sciences, School of Life Science, SOKENDAI (The Graduate University for Advanced Studies), Okazaki, Aichi 444-8585, Japan
[3]Department of Chemistry, Graduate School of Science, Kyoto University, Kyoto 606-8502, Japan
[4]RIKEN Center for Biosystems Dynamics Research, Yokohama, Kanagawa 230-0045, Japan
[5]Center for Genetic Analysis of Behavior, National Institute for Physiological Sciences, National Institutes of Natural Sciences, Okazaki, Aichi 444-8787, Japan
[6]Department of Animal Model Development, Brain Research Institute, Niigata University, Niigata 951-8585, Japan
[7]Laboratory of Animal Resources, Center for Disease Biology and Integrative Medicine, Graduate School of Medicine, The University of Tokyo, Tokyo 113-0033, Japan
[8]Centre for Discovery Brain Sciences, University of Edinburgh, Edinburgh EH16 4SB, UK
[9]Lead contact
*Correspondence: yfukata@nips.ac.jp (Y.F.), mfukata@nips.ac.jp (M.F.)
https://doi.org/10.1016/j.celrep.2021.110107

SUMMARY

What percentage of the protein function is required to prevent disease symptoms is a fundamental question in genetic disorders. Decreased transsynaptic LGI1-ADAM22 protein complexes, because of their mutations or autoantibodies, cause epilepsy and amnesia. However, it remains unclear how LGI1-ADAM22 levels are regulated and how much LGI1-ADAM22 function is required. Here, by genetic and structural analysis, we demonstrate that quantitative dual phosphorylation of ADAM22 by protein kinase A (PKA) mediates high-affinity binding of ADAM22 to dimerized 14-3-3. This interaction protects LGI1-ADAM22 from endocytosis-dependent degradation. Accordingly, forskolin-induced PKA activation increases ADAM22 levels. Leveraging a series of ADAM22 and LGI1 hypomorphic mice, we find that ~50% of LGI1 and ~10% of ADAM22 levels are sufficient to prevent lethal epilepsy. Furthermore, ADAM22 function is required in excitatory and inhibitory neurons. These results suggest strategies to increase LGI1-ADAM22 complexes over the required levels by targeting PKA or 14-3-3 for epilepsy treatment.

INTRODUCTION

Epilepsy, characterized by recurrent, unprovoked seizures, is one of the most common neurological disorders. Although various anti-epileptic drugs, mainly targeting ion channels, have been developed, more than 30% of affected individuals have inadequate control of seizures and impaired quality of life. Therefore, it is necessary to understand the pathogenic mechanisms of epilepsy and develop alternative strategies for treatment of epilepsy.

Forward genetic analyses of human pedigrees with epilepsy have identified many disease-causing mutations, most of which encode ion channel subunits that generate or modulate neuronal excitability. In addition, exome sequencing and whole-genome sequencing for individuals with epilepsy have identified epilepsy-related genes at a tremendous rate (Noebels, 2015; Steinlein, 2004). Given that disease-causing variants often or mostly cause loss-of-function (LoF) or partial LoF of the gene product, it is critical to know how much protein function is sufficient for each organ/cell to be normal. Although this question is applicable to all genetic disorders, such as cystic fibrosis and inherited epilepsy, few studies have tried to address it.

LGI1, a neuronal secreted protein, and its receptor ADAM22 are human epilepsy-related gene products that do not themselves function as ion channels. Mutations in *LGI1* cause autosomal dominant lateral temporal lobe epilepsy (Gu et al., 2002; Kalachikov et al., 2002; Morante-Redolat et al., 2002), and *Lgi1* knockout (KO) mice display generalized tonic-clonic seizures and premature death (Chabrol et al., 2010; Fukata et al., 2010; Yu et al., 2010). Compound heterozygous or homozygous mutations in *ADAM22* have been reported in individuals with early infantile epileptic encephalopathy (Maddirevula et al., 2019; Muona et al., 2016), and *Adam22* KO mice die before weaning because of multiple seizures (Sagane et al., 2005). In addition, LGI1 autoantibodies are detected most prevalently in autoimmune limbic encephalitis, which is characterized by adult-onset

memory impairment and seizures (Irani et al., 2010; Lai et al., 2010; Ohkawa et al., 2013). LGI1 autoantibodies cause neuronal hyperexcitability, decreased synaptic plasticity, and reversible memory impairment in mouse models (Kornau et al., 2020; Petit-Pedrol et al., 2018; Ramberger et al., 2020). Recent studies show that LGI1 and ADAM22 form the 2:2 LGI1-ADAM22 heterotetramer (Yamagata et al., 2018), which serves as an essential component of transsynaptic nanoarchitecture with PSD-95-family membrane-associated guanylate kinases (MAGUKs) to regulate excitatory synaptic transmission, synaptic plasticity, and neuronal excitability (Chen et al., 2021; Fukata et al., 2021). LGI1 and ADAM22 also control Kv_1 channel expression in principal excitatory neurons of the hippocampus (Fukata et al., 2010, 2021; Lugarà et al., 2020; Seagar et al., 2017) or the cortex (Zhou et al., 2018b), accounting for overexcitation of principal neurons and transmitter release, leading to epilepsy. Pathophysiological analyses revealed that pathogenic variants in *LGI1* or *ADAM22* and LGI1 autoantibodies commonly reduce the amount of LGI1-ADAM22 protein complex (Ohkawa et al., 2013; Yokoi et al., 2015). Importantly, LGI1 and ADAM22 are interdependent for their proper expression in the synapse (Yokoi et al., 2015). These studies suggest that the level of LGI1-ADAM22 protein complex is strictly regulated and could determine the seizure threshold in the brain. However, little is known about how LGI1 and ADAM22 levels are regulated and how much function of LGI1 and ADAM22 is needed for normal brain function.

Here we identify 14-3-3 proteins as a stabilizer for the functional LGI1-ADAM22 protein complex in the brain. We also determine the minimal levels of ADAM22 and LGI1 proteins that can prevent seizure phenotypes.

RESULTS

ADAM22 is quantitatively phosphorylated at Ser832 in the mouse brain

Because biogenesis of membrane proteins is often regulated posttranslationally, we first asked whether and how much ADAM22 is phosphorylated in the brain by Phos-tag SDS-PAGE analysis. ADAM22 was phosphorylated stoichiometrically in the mouse brain because ADAM22 showed a quantitative upward shift in apparent molecular weight to ~120 kDa in the Phos-tag gel, and treatment of the brain lysate with λ protein phosphatase (λPP) reversed all of the population to a lower molecular weight (~80 kDa) (Figure 1A). To determine the *in vivo* phosphorylation sites of ADAM22, ADAM22 was immunoprecipitated from the mouse brain and analyzed by mass spectrometry (MS). Several phosphorylated peptides, including Ser832, Ser855, Ser860, and Ser864, were detected (Figure 1B). Consistent with the comprehensive phosphorylation-site database PhosphoSitePlus (http://www.phosphosite.org), Ser832 was the most frequently identified phosphorylated residue. The four phosphorylated serine residues are conserved among the representative vertebrates (Figure 1C), but only Ser832 and Ser855 residues are encoded in the exons conserved among all ADAM22 splice variants (Gödde et al., 2007). We performed mutagenesis of these serine residues and expressed mutant ADAM22 proteins in rat cultured hippocampal neurons. Phos-tag SDS-PAGE showed the quantitative (~100%) shift in the mobility of wild-type (WT) ADAM22 as in the mouse brain. Importantly, mutating serine 832 to alanine (S832A) greatly reduced the shift, but other mutations hardly affected the patterns (Figure 1D). Thus, Ser832 represents the major phosphorylation site in ADAM22, and ADAM22 expressed in neurons is fully phosphorylated at Ser832. The contribution of Ser855, Ser860, or Ser864 phosphorylation to the observed shift was not apparent under the condition. A remaining, small migration shift of ADAM22-S832A in the Phos-tag gel (Figure 1D, white arrowhead) suggests their phosphorylation in neurons because the extent of shift in the Phos-tag gel often depends on the surrounding amino acid sequence.

To identify the kinase responsible for ADAM22 phosphorylation, HEK293T cells were transfected individually with 10 candidate kinases together with the cytoplasmic region (CT) of ADAM22 tagged with GFP. Western blotting using a phospho-specific antibody against ADAM22 phosphorylated at Ser832 (anti-pS832) showed that PKA robustly enhanced phosphorylation of ADAM22-S832 (Figure 1E). The ADAM22-S832 phosphorylation level was increased to more than 300% of the control level with PKA and to ~150% with other kinases, including casein kinase 2α (CK2α), Akt/protein kinase B (PKB), and protein kinase Cα (PKCα). Phosphorylation of full-length ADAM22 was enhanced by endogenous PKA activation upon forskolin treatment (Figure S1A). An *in vitro* kinase assay using recombinant proteins showed direct, robust phosphorylation of ADAM22-S832 by PKA (Figure S1B). MS analysis of *in vitro* phosphorylated ADAM22 showed that PKA phosphorylated Ser855 as well as Ser832 (Figures S1C and S1D). Given the similarity of amino acid sequences around Ser832 (-^{827}RPRSN***S***W^{833}-) and Ser855 (-^{850}RPRSN***S***T^{856}-) to the PKA consensus sequence (R-X_{1-2}-***S/T***-X), PKA is the most promising kinase for ADAM22-S832 and -S855, although we cannot exclude a role of other serine/threonine kinases in this phosphorylation event in the brain.

Phospho-deficient ADAM22 at Ser832 matures normally but is unstable in the mouse brain

To define the physiological role of ADAM22 phosphorylation at Ser832, we generated *Adam22* knockin mouse bearing a phosphorylation-deficient S832A mutation (*Adam22*^{SA}). We first confirmed loss of ADAM22-S832 phosphorylation in the *Adam22*$^{SA/SA}$ mouse brain by western blotting using an anti-pS832 antibody (Figure 2A). Phos-tag SDS-PAGE showed a great reduction in the shift of ADAM22 (ADAM22^{SA}), with slightly delayed migration. MS analysis of purified ADAM22 from the *Adam22*$^{SA/SA}$ mouse detected phosphorylated peptides at the other residues, including Ser855 (Figures S1E and S1F). Homozygous *Adam22*$^{SA/SA}$ mice appeared normal and were fertile, but protein levels of ADAM22 in the brain were reduced significantly in a mutant gene dosage-dependent manner (by ~60% in *Adam22*$^{SA/SA}$) (Figure 2B). Interestingly, LGI1 expression was also decreased by ~50%, but expression of ADAM23, PSD-95, and $Kv_{1.2}$ was not affected significantly.

We asked whether the reduced expression of ADAM22^{SA} is caused by its misfolding, impaired maturation, and/or defective intracellular trafficking. Immunohistochemistry analysis of the

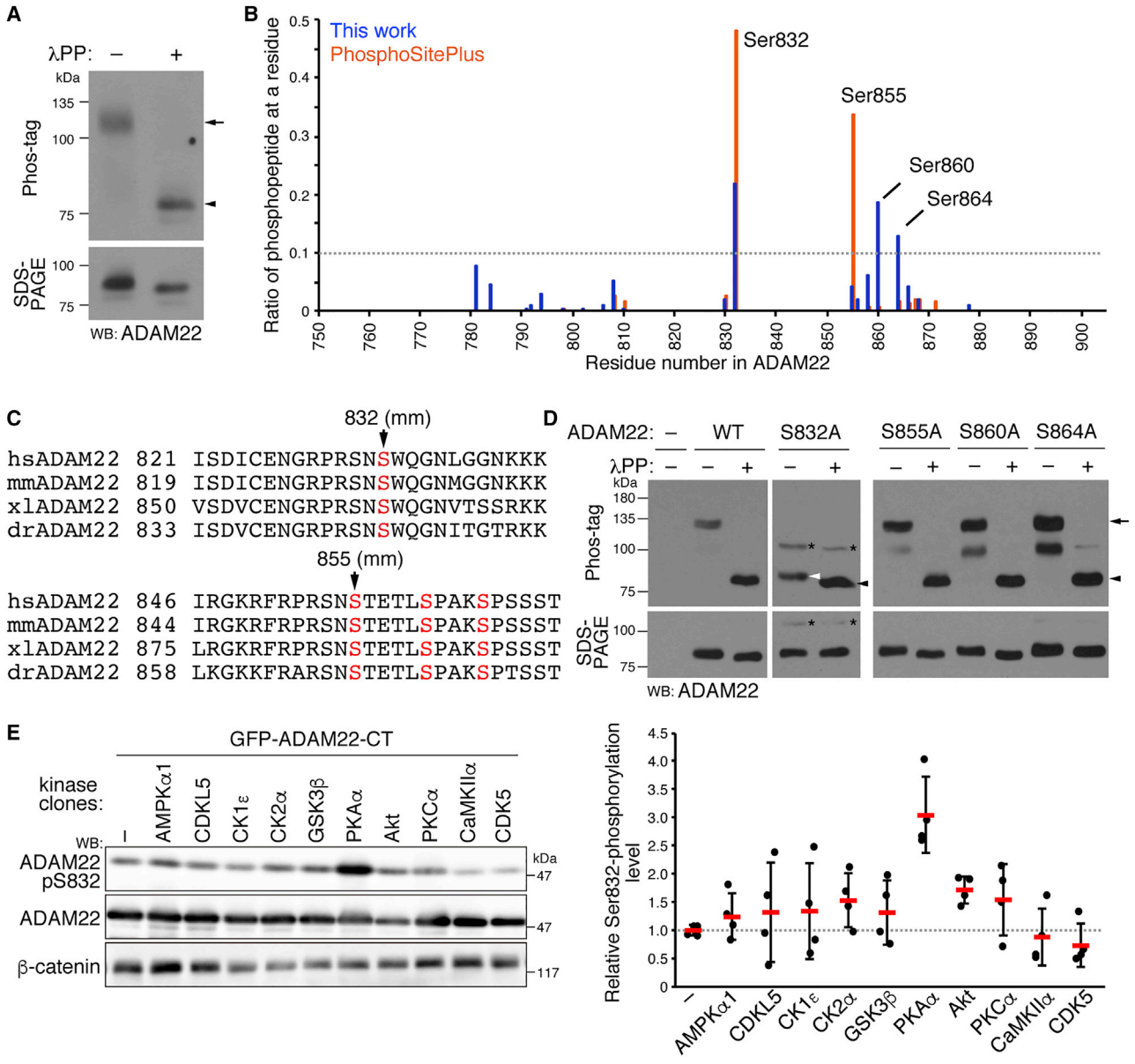

Figure 1. ADAM22 is phosphorylated quantitatively at Ser832 in the mouse brain

(A) Phos-tag SDS-PAGE and western blot (WB) of mouse whole brain lysates with anti-ADAM22 antibody show a quantitative shift of ADAM22 (arrow). Treatment with λ protein phosphatase (λPP) returns ADAM22 to an original position (arrowhead).

(B) Identification of *in vivo* phosphorylation sites of ADAM22. The height of the blue bars represents the ratio of the phosphopeptide number containing a particular phosphorylated residue to the total phosphopeptides obtained from four phosphoproteomics analyses. The height of the orange bars shows the ratio of the number of reported studies that detected the individual phosphopeptide to the total phosphoproteomics studies curated by PhosphoSitePlus.

(C) Cross-species sequence alignment of the cytoplasmic region of ADAM22, highlighting the highly phosphorylated serine residues in (B) (red). hs, *Homo sapiens*; mm, *Mus musculus*; xl, *Xenopus laevis*; dr, *Danio rerio*.

(D) Phos-tag SDS-PAGE of cell lysates from nucleofected rat hippocampal neurons. The arrow and closed arrowhead indicate the positions of phosphorylated and dephosphorylated ADAM22, respectively. Note that ADAM22-S832A still displays slightly delayed migration (white arrowhead). Asterisks, the immature form of ADAM22; WT, wild type.

(E) Individual kinase clones were transfected with the GFP-tagged ADAM22 cytoplasmic region (CT) into HEK293T cells. Ser832 phosphorylation levels were analyzed by WB using the phospho Ser832-specific ADAM22 antibody (anti-pS832). n = 4 experiments. All error bars are standard deviation (SD).

See also Figure S1.

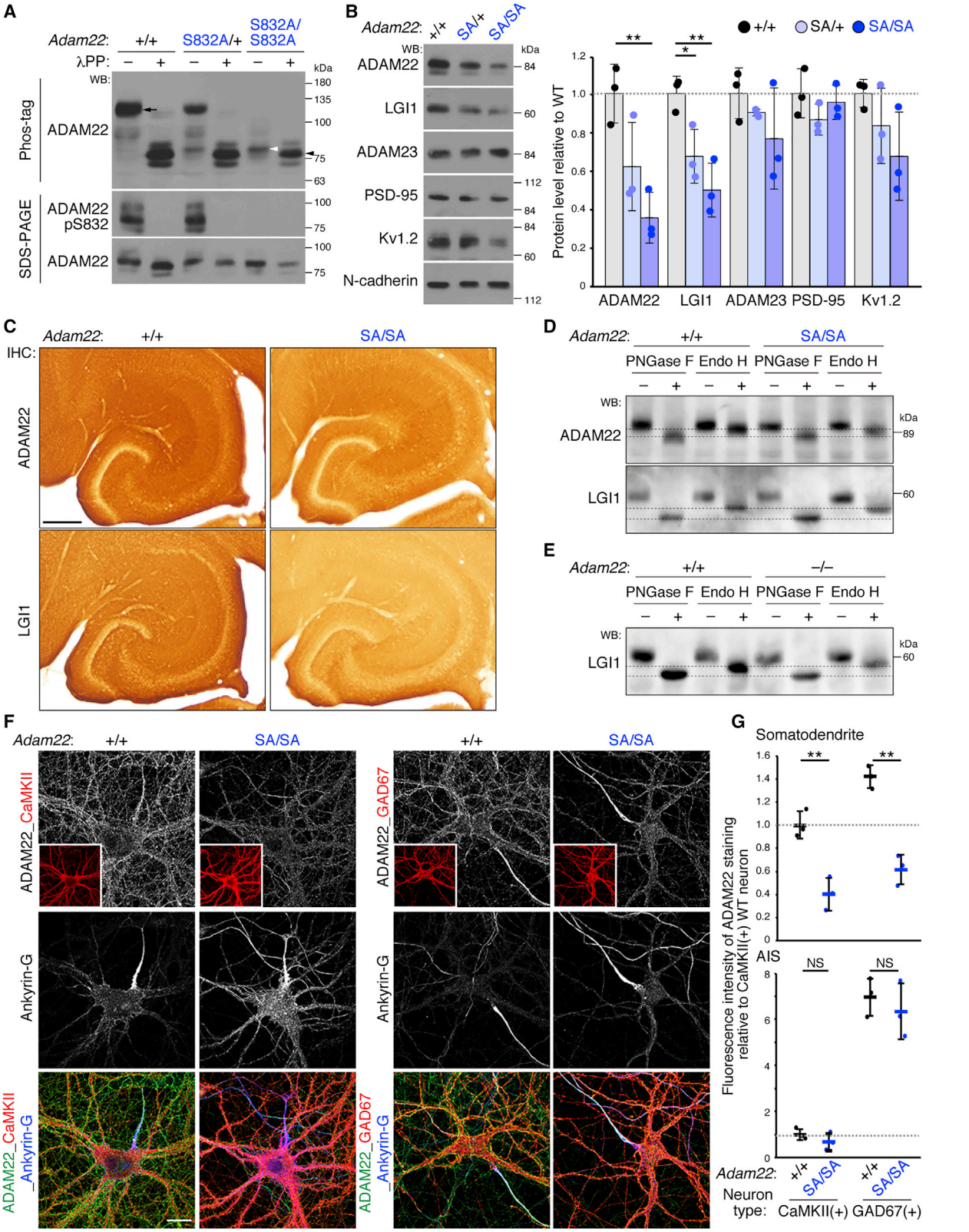

(legend on next page)

mouse brain sections showed that the overall intensity of ADAM22 staining was reduced in *Adam22*$^{SA/SA}$ mice, but the distribution pattern of ADAM22^{SA} was similar to that in the WT mouse: ADAM22 was excluded from somata and occurred in the neuropil in the hippocampus (Figure 2C). Similar results were obtained by LGI1 staining. When the brain lysate from *Adam22*$^{SA/SA}$ mice was fractionated by Triton X-100 solubility, ADAM22^{SA} was detected in the Triton X-100-insoluble fraction, suggesting its targeting to the plasma membrane (Figure S2A). We next biochemically examined the *N*-glycosylation processing of ADAM22^{SA} and LGI1 proteins. In general, glycosylation patterns are distinguished with endoglycosidase H (Endo H), which digests only immature high-mannose sugars, and peptide *N*-glycosidase F (PNGase F), which removes all *N*-linked carbohydrates. ADAM22 in the WT mouse brain was mostly resistant to Endo H and a further mobility shift of ADAM22 was observed upon PNGase F treatment (Figure 2D). ADAM22^{SA} in the brain showed behavior similar to WT ADAM22, indicating that ADAM22^{SA} becomes mature like WT ADAM22. The Endo H sensitivity of LGI1 was not changed in WT, *Adam22*$^{SA/SA}$, and even *Adam22*$^{-/-}$ mouse brains, indicating that maturation of LGI1 was not affected by ADAM22 levels (Figures 2D and 2E). These results suggest that ADAM22^{SA} normally matures and traffics to the plasma membrane.

We further analyzed ADAM22^{SA} distribution in cultured cortical neurons derived from the *Adam22*$^{SA/SA}$ mouse. WT ADAM22 was distributed along the axonal and somatodendritic membranes in Ca^{2+}/calmodulin-dependent protein kinase II (CaMKII)-positive excitatory and GAD67-positive inhibitory neurons (Figures 2F and 2G). Additionally, ADAM22 was enriched at the axon initial segment (AIS; labeled by ankyrin-G) in inhibitory neurons (Bonetto et al., 2019). Quantitative analysis showed that the overall intensity of ADAM22 was reduced significantly in excitatory and inhibitory *Adam22*$^{SA/SA}$ neurons, but the intensity in the AIS was not affected. ADAM22 enrichment in the AIS was observed similarly in parvalbumin (PV) and somatostatin (SOM)-positive inhibitory cortical neurons and was not affected (Figures S2B–S2D). Thus, ADAM22-S832 phosphorylation regulates a net amount of mature ADAM22 on the somatodendritic plasma membrane.

Phosphorylation of ADAM22-S832 protects ADAM22 from lysosomal degradation

Because the early biogenesis of ADAM22^{SA} appears normal, we next asked whether ADAM22^{SA} is unstable after its maturation. We measured the half-life of the ADAM22 protein by cycloheximide (CHX)-chase assay. WT or *Adam22*$^{SA/SA}$ cortical neurons were incubated with the translational inhibitor CHX, and cell lysates were applied to western blotting with an ADAM22 antibody. The half-life ($t_{1/2}$) of WT ADAM22 was ~77 h (Figure 3A). Importantly, the $t_{1/2}$ of ADAM22^{SA} was ~23 h, indicating that phosphorylation of ADAM22-S832 protects ADAM22 from degradation. The rapid ADAM22^{SA} degradation was mediated primarily by the lysosomal degradation pathway because ADAM22^{SA} degradation was largely blocked by treatment with leupeptin and chloroquine, inhibitors of lysosomal protein degradation (Figure 3B). MG-132 alone, an inhibitor of proteasomal proteolysis, had little effect, but when combined with leupeptin and chloroquine, MG-132 enhanced their effect, suggesting some interplay between lysosomal and proteasomal pathways for ADAM22^{SA} degradation.

Next, to examine which pool of the ADAM22 protein complexes is affected in the *Adam22*$^{SA/SA}$ mouse brain, we performed blue native (BN)-PAGE. In the WT mouse brain, ADAM22 occurs in two different protein complexes: an ~1.2-MDa supercomplex (Frank et al., 2016; Fukata et al., 2021) and a lower-molecular-weight (LMW) complex (<250 kDa) (Figure 3C). As reported previously (Fukata et al., 2021), the ~1.2-MDa supercomplex was totally dependent on the presence of LGI1, whereas the LMW complex was independent of LGI1 (WT versus *Lgi1*$^{-/-}$). Interestingly, the LMW complex of ADAM22 disappeared almost completely in the *Adam22*$^{SA/SA}$ mouse brain (Figures 3C and 3D). In contrast, the 1.2-MDa ADAM22 supercomplex was preserved preferentially, despite reducing to ~60% levels (Figures 3D and 3E). The 1.2-MDa ADAM22 supercomplex included ADAM23 and $Kv_{1.2}$ as well as LGI1 (Fukata et al., 2021), and these components were reduced similarly in the *Adam22*$^{SA/SA}$ mouse brain (Figure 3E). Given that the interaction between ADAM22 and PSD-95-family MAGUKs is essential for supercomplex formation (Fukata et al., 2021), it is conceivable that the LMW complex of ADAM22 represents a precursor or reservoir pool for the 1.2-MDa supercomplex and that non-phosphorylated ADAM22 is highly unstable at the plasma membrane unless it encounters LGI1 and PSD-95-family MAGUKs.

Ser832 phosphorylation-dependent 14-3-3 interaction stabilizes ADAM22 on the cell surface

We then asked how ADAM22 becomes unstable in the *Adam22*$^{SA/SA}$ mouse brain. We compared ADAM22-mediated protein networks of WT and *Adam22*$^{SA/SA}$ mice. Immunoprecipitation of ADAM22 from brain lysates of each genotype confirmed that ADAM22 (90 kDa) and co-purified LGI1 (60 kDa) were reduced in the *Adam22*$^{SA/SA}$ mouse. Importantly, one

Figure 2. Phosphorylation-deficient ADAM22 at Ser832 matures normally but is unstable in the mouse brain

(A) Whole-brain lysates from the *Adam22* knockin (S832A) mouse littermates were evaluated by Phos-tag SDS-PAGE (top) and WB. The arrow and closed arrowhead are as in Figures 1A and 1D. ADAM22-S832A still displays slightly delayed migration (white arrowhead). +/+, WT.

(B) Shown are quantitative WBs, with the indicated antibodies, of the forebrain lysates (P17 mice, 18 μg proteins). SA, S832A. n = 3 animals. Statistical tests used were one-way ANOVA followed by post hoc Tukey's test. *$p < 0.05$, **$p < 0.01$. All error bars are SD.

(C) Immunohistochemistry (IHC) analysis of ADAM22 and LGI1 in the hippocampus of the *Adam22*$^{SA/SA}$ mouse. Scale bar, 200 μm.

(D and E) Whole-brain lysates were treated with PNGase F or Endo H and analyzed by WB with the indicated antibodies (14 μg proteins loaded for *Adam22*$^{+/+}$ mice and 35 μg for *Adam22*$^{SA/SA}$ [D] and 20 μg for *Adam22*$^{+/+}$ and 60 μg for *Adam22*$^{-/-}$ [E]).

(F and G) Cultured cortical neurons (20–25 days *in vitro* [DIV]) derived from *Adam22*$^{SA/SA}$ mice were stained with the indicated antibodies. AIS, axon initial segment. Scale bar, 10 μm. Fluorescence intensities of ADAM22 are quantified (G). n = 3 experiments. Two-tailed Student's t test. **$p < 0.01$; NS, not significant. All error bars are SD.

See also Figure S2.

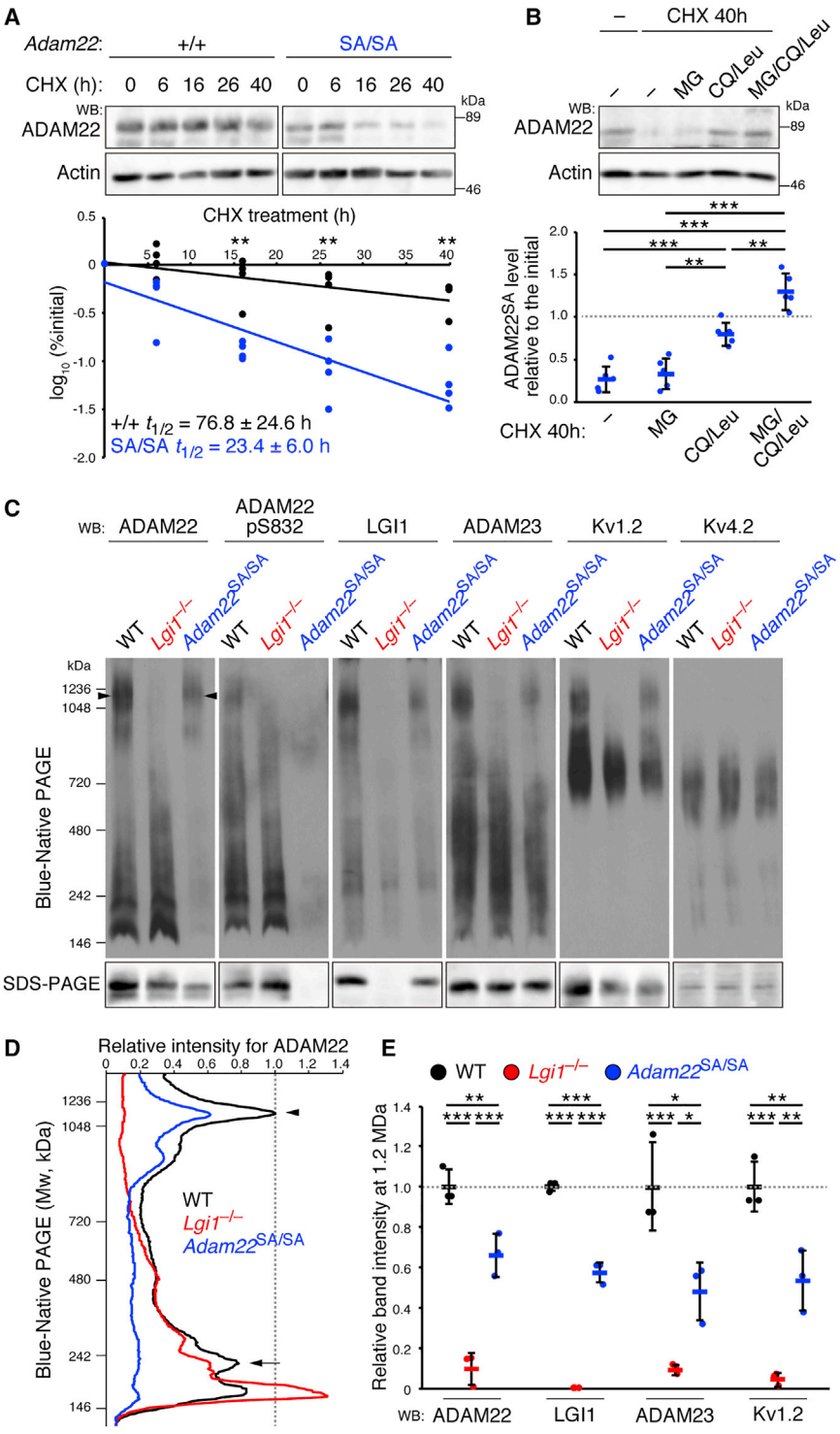

Figure 3. Phosphorylation of ADAM22-S832 protects ADAM22 from lysosomal degradation

(A) Mouse cortical neurons (6 DIV) from *Adam22*$^{SA/SA}$ or WT mice were treated with cycloheximide (CHX; 20 μg/mL) for the indicated periods, and lysates were subjected to WB. $t_{1/2}$, the half-life of ADAM22 protein. n = 4 experiments. Two-tailed Student's t test. **p < 0.01.

(B) *Adam22*$^{SA/SA}$ cortical neurons were co-treated with CHX plus MG-132 (MG; 10 μM) or leupeptin (Leu, 100 μM)/chloroquine (CQ, 200 μM) for 40 h, followed by WB. Remaining ADAM22^{SA} proteins after the treatment are quantified (bottom). n = 5 experiments. Statistical tests used were one-way ANOVA followed by post hoc Turkey's test. **p < 0.01, ***p < 0.001. All error bars are SD.

(C–E) Equal amounts of brain extracts from WT (black), *Lgi1*$^{-/-}$ (red), and *Adam22*$^{SA/SA}$ (blue) mice (P17) were analyzed by BN-PAGE and WB (C). Representative densitometric intensity profiles for ADAM22 are shown (D). Band intensities for the constituents of the 1.2-MDa complex are quantified (E). Arrowhead, 1.2-MDa complex; arrow, LMW (<250 kDa). n = 3 experiments. Statistical tests used were one-way ANOVA followed by post hoc Tukey's test. *p < 0.05, **p < 0.01, ***p < 0.001. All error bars are SD.

band with a molecular mass of ~28 kDa (p28) disappeared specifically in the *Adam22*$^{SA/SA}$ mouse (Figure 4A). MS analysis revealed that p28 was 14-3-3 isoforms (ε, ζ, θ, γ, β, and η), and western blotting showed a great reduction of 14-3-3 binding in the *Adam22*$^{SA/SA}$ mouse brain (Figure 4B). This indicates that ADAM22 binds to 14-3-3 in a Ser832 phosphorylation-dependent manner. In contrast, ADAM22^{SA} retains the binding to LGI1, $Kv_{1.2}$, and PSD-95 (Figure 4B).

Because the synaptic function of ADAM22 requires its binding to PSD-95-like MAGUKs (Chen et al., 2021; Fukata et al., 2021), we examined the mode of interactions between ADAM22, 14-3-3, and PSD-95. We took advantage of the *Adam22* knockin mouse, in which ADAM22 is fused with a tandem affinity tag composed of FLAG, AU1, and hemagglutinin (HA) (referred as to FAH tag) (Fukata et al., 2021). When ADAM22-FAH was immunoaffinity purified by anti-FLAG agarose from the mouse brain, ADAM22-FAH-containing protein complexes included PSD-95 and 14-3-3 as well as LGI1 (Figure S3). Then PSD-95 was reprecipitated from the immunoaffinity purification (IAP) eluate by an anti-PSD-95 antibody (second immunoprecipitation [IP]). Western blotting revealed that 14-3-3 as well as ADAM22-LGI1 were enriched with PSD-95. This result indicates that PSD-95 and 14-3-3 bind to ADAM22 without competition, constituting the 14-3-3-ADAM22-PSD-95 complex as well as the 14-3-3-ADAM22 complex.

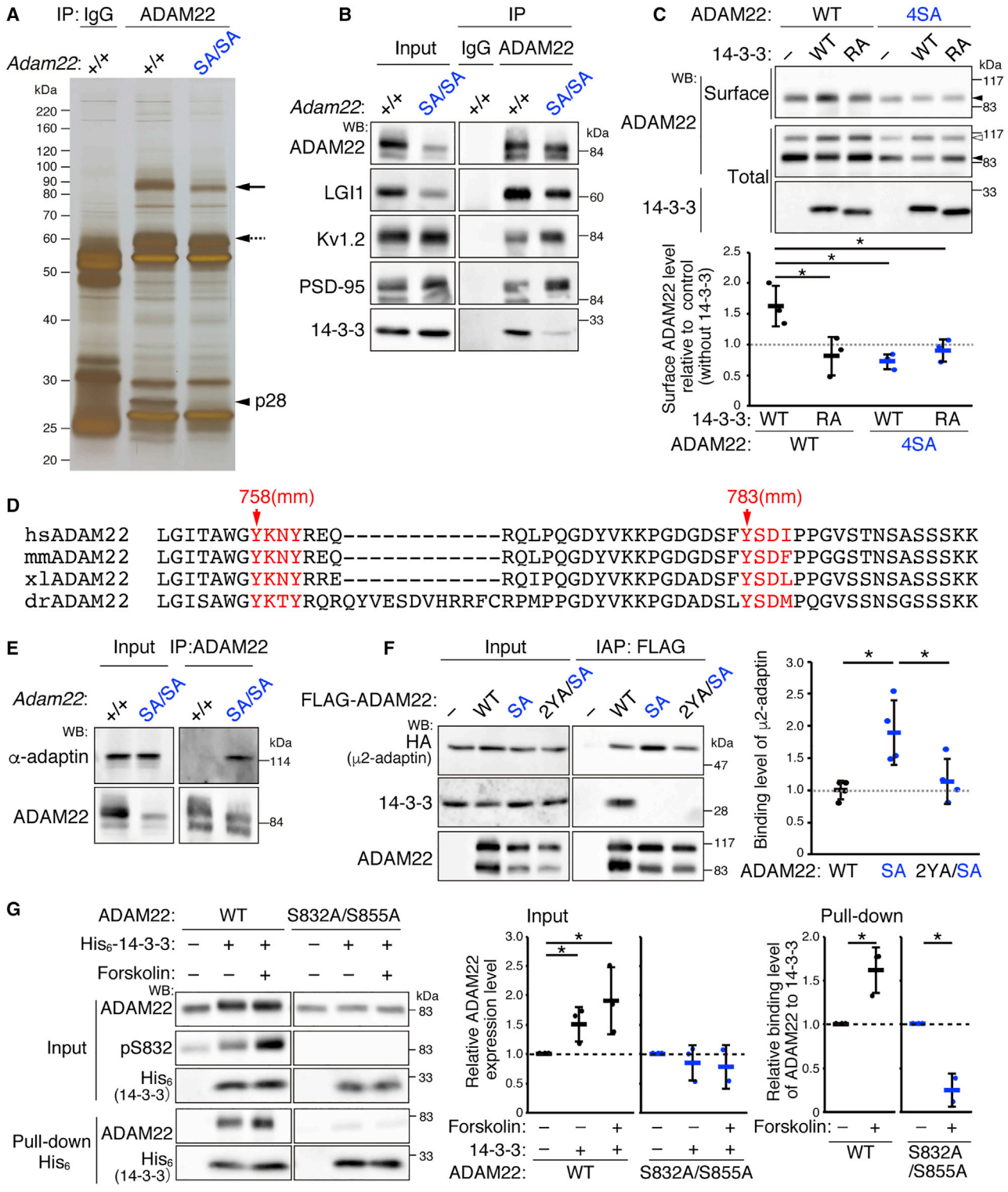

Figure 4. The Ser832 phosphorylation-dependent 14-3-3 interaction stabilizes ADAM22 on the cell surface

(A) Silver staining of ADAM22 immunoprecipitates from the indicated mouse brains. The bands with molecular masses of ~90, ~60 and ~28 kDa, indicated by an arrow, dotted arrow, and arrowhead, respectively, correspond to ADAM22, LGI1, and 14-3-3, respectively. IP, immunoprecipitation.

(B) WBs of the ADAM22 immunoprecipitates with the indicated antibodies.

(legend continued on next page)

14-3-3 family proteins are ubiquitously expressed phosphoprotein-binding proteins and participate in regulation of a wide range of cellular processes (Bridges and Moorhead, 2005; Smith et al., 2011). 14-3-3 proteins exist as homodimers or heterodimers and bind to more than 100 clients and regulate their activity, intracellular transport, and stability. Although binding of 14-3-3 to ADAM22 has been reported previously (Fukata et al., 2010, 2021; Gödde et al., 2006; Zhu et al., 2003), the physiological role of this interaction remains incompletely understood. To examine whether 14-3-3 regulates the level of ADAM22, especially mature ADAM22, we performed a cell surface biotinylation assay of transfected COS7 cells (Figure 4C). 14-3-3 coexpression increased the level of cell surface biotinylated ADAM22. This enhanced effect depends on the specific interaction between phosphorylated ADAM22 and 14-3-3 because (1) 14-3-3 R56A/R60A (RA), which cannot bind to the phospho-clients, had no effect, and (2) 14-3-3 did not increase phosphorylation-deficient ADAM22-S832A/S855A/S860A/S864A (4SA) cell surface expression. This positive effect of 14-3-3 could result from an increase in intracellular trafficking by masking the endoplasmic reticulum (ER) retention signal of clients (Godde et al., 2006) or a decrease in endocytosis-mediated internalization of clients. Because we observed no retained $ADAM22^{SA}$ protein in the ER or cell body (Figures 2C, 2D, and 2F), and lysosomal degradation of $ADAM22^{SA}$ was accelerated in neurons (Figure 3B), we pursued the latter possibility. We noted that two Yxxϕ motifs (-^{758}YKNY^{761}- and -^{783}YSDF^{786}- in mice; ϕ represents a bulky hydrophobic residue), the consensus sequences for the binding to AP2 μ2 subunit, are evolutionarily conserved in the cytoplasmic region of ADAM22 (Figure 4D). Interestingly, α-adaptin (α subunit of AP2) binding with ADAM22 was not readily detected in the WT mouse brain, whereas AP2 bound more abundantly to ADAM22 in the *Adam22*$^{SA/SA}$ mouse (Figure 4E). The increased interaction between AP2 and $ADAM22^{SA}$ is specific because binding of the μ2 subunit of AP2 to $ADAM22^{SA}$ was canceled by the mutations (2YA) in the Yxxϕ motifs in heterologous cells (Figure 4F). μ2-adaptin apparently bound to WT ADAM22 in HEK293T cells (Figure 4F), inconsistent with the negligible binding in the normal brain (Figure 4E). This difference might be due to overexpression of ADAM22 in HEK293T cells, which could outnumber endogenous 14-3-3 proteins in cells, allowing 14-3-3-free WT ADAM22 to bind to μ2-adaptin.

Furthermore, we examined whether PKA, which phosphorylates Ser832 and Ser855 of ADAM22, regulates these processes. Consistently with Figure 4B, the S832A mutation of ADAM22 greatly reduced ADAM22 binding to His_6-14-3-3 in HEK293T cells (Figure S4). The S855A mutation also significantly reduced 14-3-3 interaction, and the double mutation S832A/S855A further reduced this interaction. These results suggest a primary role of Ser832 phosphorylation and a cooperative role of Ser855 phosphorylation in the ADAM22-14-3-3 interaction. We then found that PKA activation by forskolin, which elevates S832 phosphorylation, increased the 14-3-3 interaction and the expression level of WT ADAM22 (Figure 4G). These effects of PKA activation were canceled completely with $ADAM22^{S832A/S855A}$. These results suggest that the interaction of phosphorylated ADAM22 with 14-3-3 protects ADAM22 from AP2 binding and subsequent clathrin-mediated endocytosis and lysosomal degradation.

Structural basis for the interaction of phosphorylated ADAM22 with 14-3-3

Next we investigated the structural basis of the ADAM22-14-3-3 interaction. Importantly, two phospho-serine motifs of ADAM22, ^{829}RSN**pS**WQ^{834} and ^{852}RSN**pS**TE^{857}, fall into the consensus motif for 14-3-3 binding (-RSX**pS**XP-) (Figure 1C). We asked whether a 14-3-3 dimer, which contains two binding grooves for phospho-serine/threonine motifs, binds to either motif (pS832 or pS855) on two independent ADAM22 molecules or two tandem motifs (pS832 and pS855) on a single ADAM22 molecule. We performed isothermal titration calorimetry (ITC) experiments to measure the stoichiometry and binding affinity between phosphorylated ADAM22 peptides and a 14-3-3ε dimer. Two ADAM22 synthetic peptides, a singly phosphorylated peptide (pS832 alone, ^{827}RPRSN**pS**WQGN^{836}, referred as to pADAM22) and a doubly phosphorylated peptide (pS832 and pS855, ^{827}RPRSN**pS**WQGNMGGNKKKIRGKRFRPRSN**pS**TE^{857}, ppADAM22), were examined. pADAM22 bound to 14-3-3ε with $\sim$1:1 stoichiometry (N-value = 1.14, two pADAM22 per one 14-3-3ε dimer) and a K_d of 6.3 μM (Figure 5A). In contrast, the stoichiometry of the ppADAM22 to 14-3-3ε was apparently less than that of pADAM22 and close to 0.5 (N-value = 0.683), suggesting that one ppADAM22 peptide binds to one 14-3-3ε dimer (Figure 5B). The affinity of ppADAM22 for 14-3-3ε (K_d, 25.5 nM) was increased robustly about 250-fold compared with that of pADAM22. Thus, the adjacent phosphoserine motifs (pS832 and pS855) of ADAM22 simultaneously occupy the two binding pockets of a 14-3-3 dimer, resulting in a high-affinity complex of one ADAM22 and two 14-3-3 proteins. Similar

(C) The cell surface biotinylation assay in transfected COS7 cells. 4SA, S832A/S855A/S860A/S864A; RA, R56A/R60A. Open and closed arrowheads indicate the immature and mature forms of ADAM22, respectively. The cell surface ADAM22 levels are quantified (bottom). n = 3 experiments. Statistical tests used were one-way ANOVA followed by post hoc Tukey's test. *p < 0.05. All error bars are SD.

(D) The AP2-binding, endocytic motif "Yxxϕ" is conserved in the ADAM22 cytoplasmic region among vertebrates. The residues matching the Yxxϕ motif are highlighted.

(E) ADAM22 immunoprecipitates from WT and *Adam22*$^{SA/SA}$ mouse brains were analyzed with an anti-α-adaptin antibody.

(F) ADAM22 mutants at the tyrosine residues of the Yxxϕ motifs (2YA, Y758A/Y783A) and/or $ADAM22^{S832A}$ were co-expressed with HA-tagged μ2-adaptin in COS7 cells, and the interaction of ADAM22 with μ2-adaptin was assessed (IAP, immunoaffinity purification). Binding of μ2-adaptin to ADAM22 is quantified (right). n = 4 experiments. Statistical tests used were one-way ANOVA followed by post hoc Turkey's test. *p < 0.05. All error bars are SD.

(G) Transfected HEK293T cells were treated with forskolin (50 μM, 15 h) or left untreated, and binding of ADAM22 to His_6-tagged 14-3-3 was analyzed (left). ADAM22 expression levels in input (center) and binding of ADAM22 to 14-3-3 (right, pull-down) are quantified. n = 2 or 3 experiments. Statistical tests used were Kruskal-Wallis one-way ANOVA followed by post hoc Steel's test for input samples and one-tailed, one-sample Student's t test for pull-down samples. *p < 0.05. All error bars are SD.

See also Figures S3 and S4.

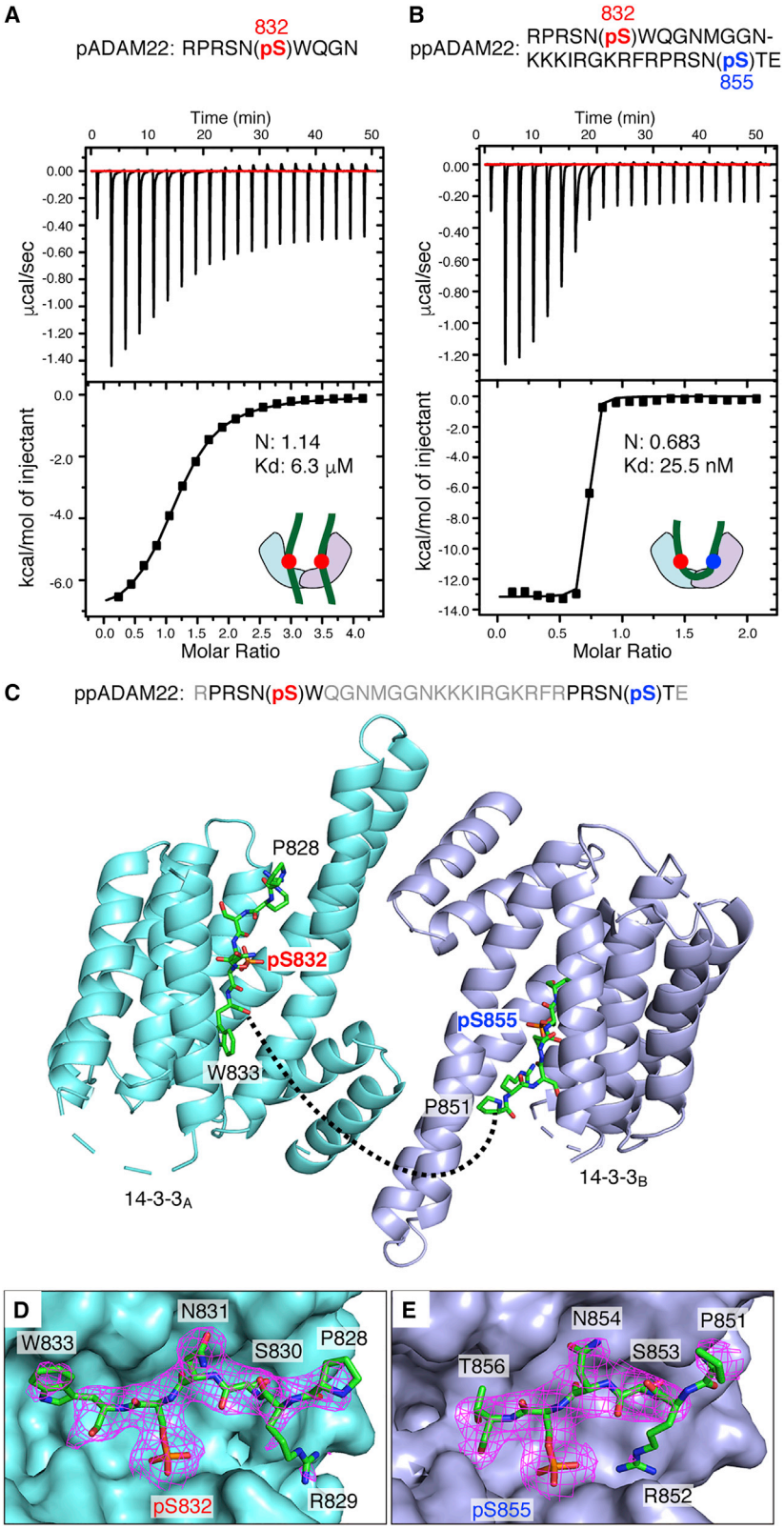

Figure 5. Structural basis for the interaction of phosphorylated ADAM22 with 14-3-3

(A) and (B) ITC titrations of 1.0 mM singly phosphorylated (pS832 (A)) or 0.5 mM doubly phosphorylated (pS832 and pS855 (B)) peptide into 50 µM 14-3-3ε. Listed for each experiment are the dissociation constant (K_d) and binding stoichiometry (N) derived from fitting of the binding isotherm.

(C) The crystal structure of a 14-3-3ζ dimer in complex with the doubly phosphorylated peptide (ppADAM22). In the sequence diagram, the portions of the peptides observed in the structures are shown in black, and the phosphorylation sites are highlighted in red and blue, whereas unresolved amino acids are shown in gray. The dashed line shows amino acid residues connecting two binding sites.

(D and E) Close-up views of the binding pockets of 14-3-3ζ and corresponding $2F_o–F_c$ electron density maps of the ADAM22 peptide (red mesh, contoured at 1.0 σ level).

See also Figure S5 and Table S1.

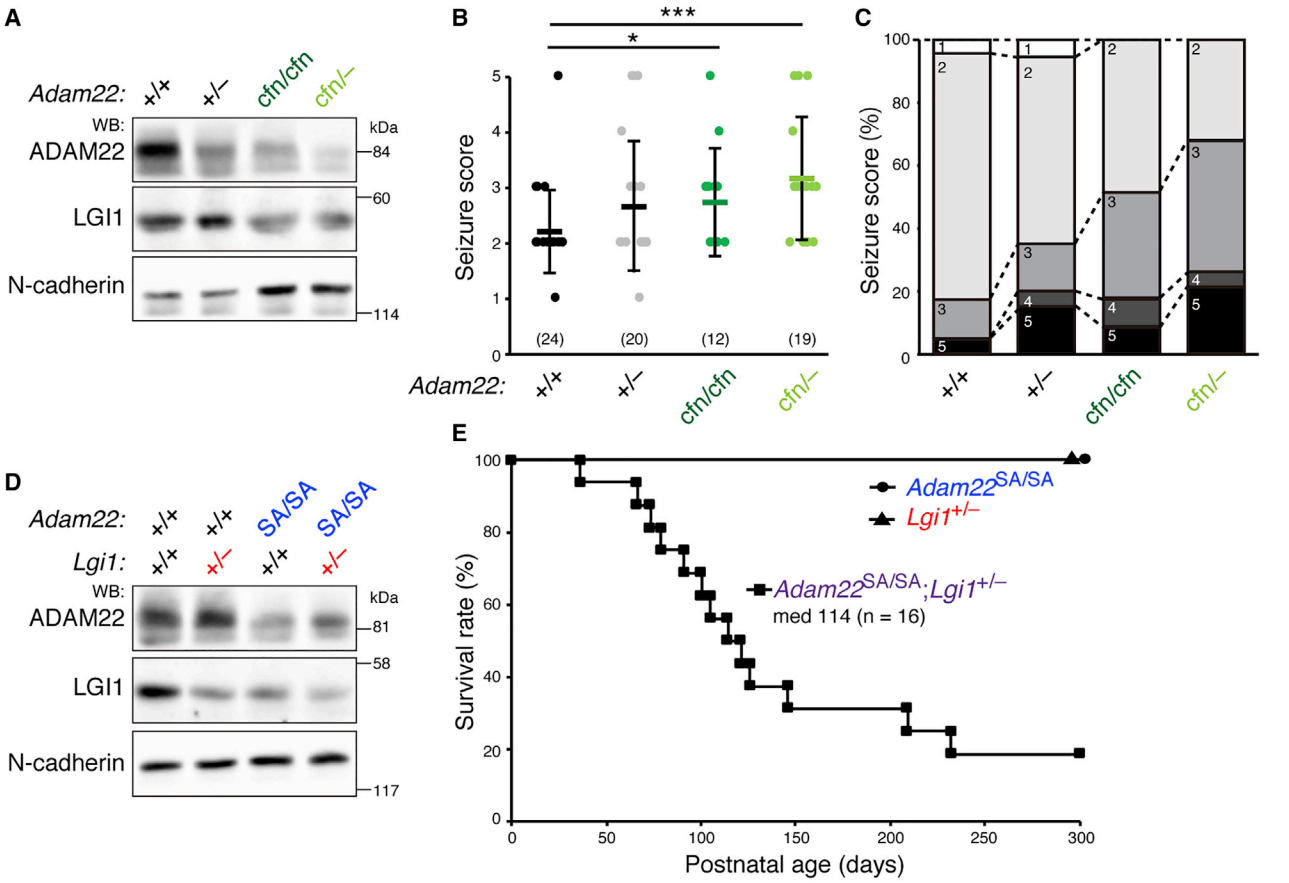

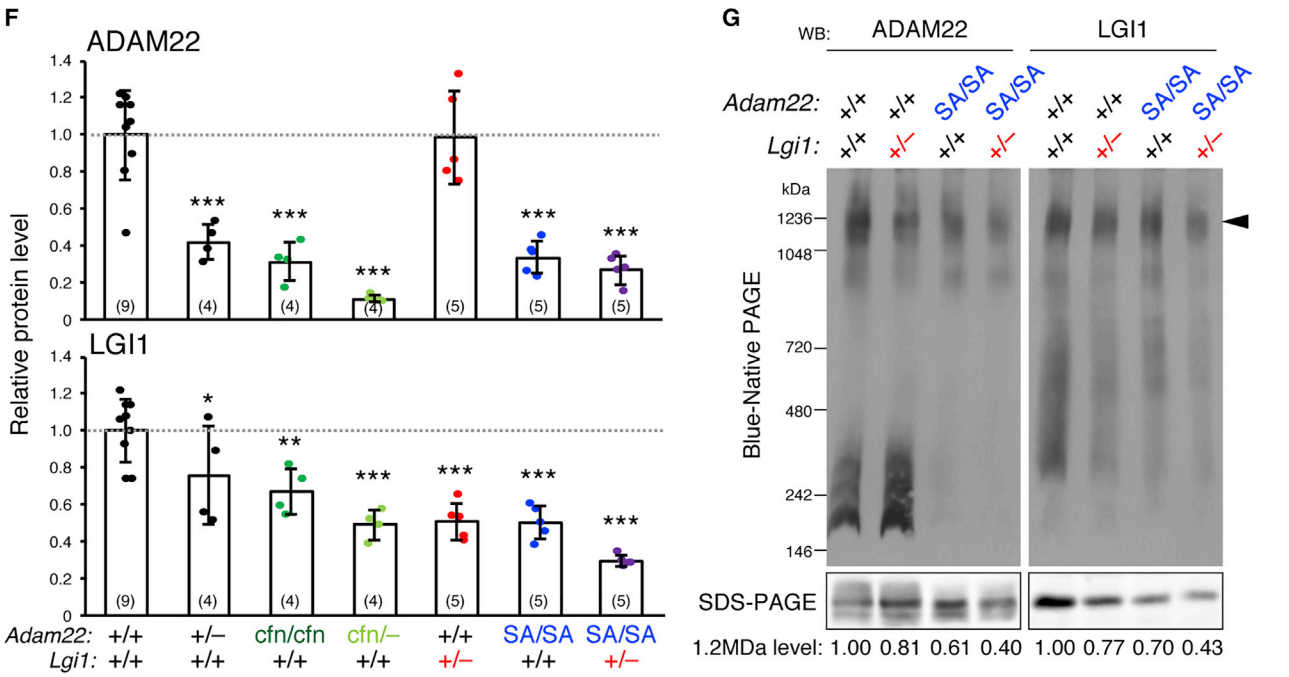

(legend on next page)

tandem repeats for 14-3-3 binding sites have been reported in PKCε (Kostelecky et al., 2009), IRSp53 (Kast and Dominguez, 2019), cRAF (Molzan and Ottmann, 2012), and CFTR (Stevers et al., 2016).

Further, we determined the crystal structure of the ppADAM22-bound 14-3-3ζ dimer at 2.75-Å resolution (Figures 5C, 5D, 5E, and S5; Table S1). The electron density map revealed two phosphoserine-containing motifs (-PRSN**pS**-) of ppADAM22. As observed in the previously reported structure of the phosphopeptide-bound 14-3-3 protein (Yaffe et al., 1997), the phosphate group of the phosphorylated serine side chain engages a conserved triad of two arginine residues and a tyrosine residue (Arg56, Arg127, and Tyr128) of 14-3-3ζ. On the other hand, the linker between two phosphorylation sites in ppADAM22 (from Gln834 to Arg850) was unresolved. Such a problem is often confronted in structural characterization of the 14-3-3 complex with a doubly phosphorylated peptide because the low-complexity region between tandem phospho-sites is usually disordered. Nevertheless, it is conceivable that dual phosphorylation-mediated binding of dimerized 14-3-3 competitively inhibits binding of AP2 to ADAM22 to prevent endocytosis of ADAM22.

ADAM22 and LGI1 levels to suppress lethal seizures in mice

Individuals with ADAM22-related encephalopathy carrying the homozygous or compound heterozygous LoF mutations are severely affected, whereas their parents with a heterozygous mutation do not show neurological symptoms (Maddirevula et al., 2019; Muona et al., 2016). All *Adam22*$^{-/-}$ mice showed premature death because of epileptic seizures (Sagane et al., 2005), and *Adam22*$^{+/-}$ and *Adam22*$^{SA/SA}$ mice, which express ADAM22 at ~40% of the protein levels of WT mice (Figures 2B, 6A, 6D, and 6F), displayed neither obvious spontaneous seizures nor sudden death. Therefore, we asked what percentage of the ADAM22 protein level is sufficient to prevent epilepsy or to be restored. We established a series of mouse lines that express ADAM22 at various protein levels: *Adam22*$^{+/+}$, *Adam22*$^{+/-}$, *Adam22*$^{SA/SA}$, *Adam22*$^{cfn/cfn}$ (conditional FRT-flanked neomycin [cfn]), and *Adam22*$^{cfn/-}$ (Figures 6A, 6D, and 6F). Mice with the *Adam22*^{cfn} allele (Ozkaynak et al., 2010) showed reduced *Adam22* gene expression, an effect observed often (Tokumasu et al., 2016). We therefore used the *Adam22*^{cfn} allele as an *Adam22* hypomorphic allele. We examined the relationship between protein levels of ADAM22 and seizure phenotypes among genotypes. *Adam22*$^{cfn/cfn}$ mice expressed ADAM22 at ~30% levels, and *Adam22*$^{cfn/-}$ mice, which have *Adam22*^{cfn}- and *Adam22*-null alleles, expressed it at ~10% levels (Figures 6A and 6F). They did not show obvious spontaneous seizures, suggesting that 10% of residual ADAM22 levels are sufficient to suppress lethal seizure events in mice. Importantly, seizure susceptibility to pentylenetetrazole (PTZ), a γ-aminobutyric acid $(GABA)_A$ receptor antagonist (Yokoi et al., 2015), was elevated as the expression level of ADAM22 was decreased (Figures 6B and 6C). A significantly greater fraction of *Adam22*$^{cfn/-}$ mice (average score, 3.2; n = 19) responded to a single injection of PTZ (35 mg/kg) than WT *Adam22*$^{+/+}$ mice (score 2.2; n = 24; $p < 0.001$) (Figure 6B). Generalized clonic or tonic seizures (seizure score, 4 or 5) were observed more frequently in *Adam22*$^{cfn/-}$ mice (26%) compared with WT mice (4%) (Figure 6C). *Adam22*$^{cfn/cfn}$ mice showed modestly increased seizure susceptibility to PTZ (score, 2.8, n = 12, $p < 0.05$), with more frequent seizure behavior (seizure score > 3) than WT mice. Thus, when ADAM22 protein levels are below 30%, the brain becomes more susceptible to seizure generation.

We next asked how much the LGI1 protein level contributes to the increased seizure susceptibility of *Adam22*$^{cfn/-}$ mice because (1) heterozygous *Lgi1* KO mice(*Lgi1*$^{+/-}$) similarly show increased seizure susceptibility but no spontaneous seizures (Fukata et al., 2010), and (2) LGI1 and ADAM22 are interdependent for their proper expression (Fukata et al., 2010; Yokoi et al., 2015). Interestingly, the LGI1 level in *Adam22*$^{cfn/-}$ mice was similar to that in *Lgi1*$^{+/-}$ mice (i.e., at ~50% levels) (Figures 6A, 6D, and 6F). We then obtained *Adam22*$^{SA/SA}$;*Lgi1*$^{+/-}$ mice, which have *Adam22*^{SA} alleles in addition to a heterozygous *Lgi1* KO allele. The mice expressed LGI1 at ~30% levels (Figures 6D and 6F) and displayed spontaneous generalized seizures causing sudden death (median lifespan, 114 days; Figure 6E; Video S1). Thus, alterations of LGI1 levels could more sensitively affect the severity of seizure phenotypes than alterations of ADAM22 levels. Our combinatorial analysis revealed that ~10% of ADAM22 and ~50% of LGI1 levels are sufficient to prevent lethal epilepsy in mice.

Concomitant with reduction of LGI1 and ADAM22 levels, $Kv_{1.2}$ expression levels were decreased in *Adam22* hypomorphic mouse lines (Figure S6) whereas $GABA_A$ receptor expression levels were not. $Kv_{1.2}$ expression levels showed a stronger positive correlation with ADAM22 expression levels than with LGI1.

Figure 6. The ADAM22 and LGI1 levels to suppress lethal seizures in mice

(A) A representative WB (top) showing ADAM22 protein levels in the mouse forebrain lysate of each genotype (P16–P18). The LGI1 levels analyzed are shown (center). cfn, conditional FRT-flanked neomycin.

(B and C) Responses of 1-month-old mice with the indicated genotypes to a single PTZ injection (35 mg/kg). Seizure scores: 0, no reaction; 1, twitching; 2, myoclonic body jerks; 3, clonic forelimb convulsions; 4, generalized clonic convulsions, turn over into side position; 5, generalized tonic convulsions. The number of animals examined is indicated on the graph (B). Statistical tests used were Kruskal-Wallis test followed by post hoc Steel's test. *$p < 0.05$, ***$p < 0.001$. All error bars are SD.

(D and E) LGI1 protein level in the forebrain lysate is further decreased in *Adam22*$^{SA/SA}$;*Lgi1*$^{+/-}$ mice compared with *Lgi1*$^{+/-}$ or *Adam22*$^{SA/SA}$ mice (D). Kaplan-Meier survival plots of *Lgi1*$^{+/-}$, *Adam22*$^{SA/SA}$, and *Adam22*$^{SA/SA}$;*Lgi1*$^{+/-}$ mice are shown in (E).

(F) ADAM22 and LGI1 protein levels in a series of mutant mouse brains examined in (A) and (D). The number of animals examined is indicated on the graph. Statistical tests used were one-way ANOVA followed by post hoc Dunnett's test. *$p < 0.05$, **$p < 0.01$, ***$p < 0.001$. All error bars are SD.

(G) BN-PAGE and WB of brain extracts (P100) show that the 1.2-MDa ADAM22 supercomplex is further decreased in the *Adam22*$^{SA/SA}$;*Lgi1*$^{+/-}$ mouse brain (arrowhead) compared with *Lgi1*$^{+/-}$ or *Adam22*$^{SA/SA}$ mice. 1.2-MDa complex levels relative to that in the WT are indicated at the bottom.

See also Figure S6.

Consistently, BN-PAGE showed that the 1.2-MDa supercomplex containing ADAM22 and LGI1 in the *Adam22*$^{SA/SA}$;*Lgi1*$^{+/-}$ mouse brain was decreased further by ~60% (Figure 6G). As in the *Adam22*$^{SA/SA}$ mouse brain (Figure 3C), the 1.2-MDa complex was preferentially maintained rather than the LMW complex, suggesting that the 1.2-MDa ADAM22 complex represents the functional complex and dose-dependently controls seizure phenotypes of the mice (Figure 6G). The deteriorated phenotypes in *Adam22*$^{SA/SA}$;*Lgi1*$^{+/-}$ mice (Figure 6E) indicate that post-translational regulation of ADAM22 is critical to maintain the levels of functional LGI1-ADAM22 complexes and, therefore, to prevent seizures.

ADAM22 and LGI1 functions in excitatory and inhibitory neurons are essential for seizure suppression

We then asked which types of neurons in the brain need the ADAM22 function. We took the conditional KO approach mainly under the *Adam22*$^{cfn/cfn}$ hypomorphic background, because ADAM22 levels were reduced comparably in *Adam22*$^{cfn/cfn}$ and *Adam22*$^{flox/flox}$ mice (STAR Methods; Figure S7A). Using an *Emx1-Cre* driver line, we first deleted the *Adam22* gene in forebrain neural progenitor cells, the precursors of neocortical and hippocampal glutamatergic neurons at embryonic day 10.5 (E10.5) (Kassai et al., 2008). Western blotting confirmed specific deletion of ADAM22 in the hippocampus, cortex, and olfactory bulb but not in the thalamus and cerebellum (Figure 7A). Lifespan analysis revealed that all *Adam22*$^{cfn/cfn}$;*Emx1*$^{Cre/+}$ mice died prematurely around post-natal day 18 (P18) (Figure 7B), with a survival curve similar to that of *Lgi1*$^{-/-}$ mice with lethal epilepsy (Fukata et al., 2010). Importantly, selective deletion of *Adam22* in GABAergic inhibitory neurons using a *VGAT-Cre* driver also caused premature death (median lifespan, 28 days). Similar results were obtained under the *Adam22*$^{flox/flox}$ hypomorphic background (Figures S7B and S7C). To further narrow down the inhibitory neuron subtypes, we selected *PV-Cre* and *SOM-Cre* drivers, representing about 70% of neocortical inhibitory neurons (Tremblay et al., 2016). *Adam22*$^{cfn/cfn}$;*PV*$^{Cre/+}$ mice and *Adam22*$^{cfn/cfn}$;*SOM*$^{Cre/+}$ mice looked normal, but *Adam22*$^{cfn/cfn}$;*PV*$^{Cre/+}$;*SOM*$^{Cre/+}$ mice died suddenly after ~P50 (Figure 7C), suggesting roles of ADAM22 in perisomatic (by PV neurons) and dendritic (by SOM neurons) inhibition onto pyramidal neurons. These results indicate that ADAM22 expression in excitatory and inhibitory neurons is essential for mouse survival without epilepsy.

Finally, we asked the same for LGI1 expression. A previous study using *Lgi1* conditional KO mice showed that loss of LGI1 in forebrain glutamatergic neurons, but not in PV-positive interneurons, causes lethal epileptic seizures (Boillot et al., 2014). Here we took an inverse, "transgenic rescue" approach using cell-type-specific promoters. So far, we reported that the neuronal expression of LGI1 under control of a neuron-specific *Thy1* promoter (a mouse with a transgenic allele is referred as to a *Thy1-Lgi1*$^{Tg/+}$ mouse) completely rescues the epileptic phenotype of *Lgi1*$^{-/-}$ mice (Fukata et al., 2010). We selected a *VGAT* promoter to specifically express LGI1 in GABAergic inhibitory neurons. *VGAT* promoter-induced LGI1 expression significantly prolonged the lifespan of *Lgi1*$^{-/-}$ mice (Figures 7D and S8), indicating an important role of LGI1 secreted from inhibitory neurons. This suggests that the complete rescue in *Lgi1*$^{-/-}$;*Thy1-Lgi1*$^{Tg/+}$ is attributed to LGI1 secreted from not only excitatory but also inhibitory neurons.

To further narrow down the excitatory neuron types responsible for lethal epilepsy in *Lgi1*$^{-/-}$ mice, we focused on the hippocampus, where seizure activities originate in *Lgi1*$^{-/-}$ mice (Chabrol et al., 2010; Fukata et al., 2021). Because LGI1 mRNA is highly expressed in the dentate granule cells and CA3 pyramidal neurons (Fukata et al., 2006; Ohkawa et al., 2013), LGI1 expression was driven in these principal neurons, using the *prospero homeobox 1* (*Prox1*) promoter for dentate granule cells and the glutamate receptor *KA-1* (*KA1*) promoter for CA3 pyramidal neuron-specific expression (Figures S8A and S8B). We confirmed the specific patterns of LGI1 protein secreted from the targeted neurons, occupying their defined axonal and dendritic territories (Figures 7E and S8C; Lovero et al., 2015). Transgenic rescue experiments showed that expression of LGI1 in dentate granule cells or CA3 pyramidal neurons (*Lgi1*$^{-/-}$;*Prox1-Lgi1*$^{Tg/Tg}$ or *Lgi1*$^{-/-}$;*KA1-Lgi1*$^{Tg/Tg}$ mice) was not sufficient to rescue *Lgi1*$^{-/-}$ mice and allowed survival that was prolonged only by a few days (Figure 7D). When LGI1 was expressed in dentate granule cells and inhibitory neurons (*Lgi1*$^{-/-}$;*Prox1-Lgi1*$^{Tg/Tg}$;*VGAT-Lgi1*$^{Tg/Tg}$), the lifespan of *Lgi1*$^{-/-}$ mice was prolonged for ~14 days, suggesting that LGI1 secreted from dentate excitatory and inhibitory neurons is involved in the severity of epilepsy.

DISCUSSION

In this study, we find that PKA-mediated dual phosphorylation of ADAM22 establishes a stable interaction with 14-3-3 to protect LGI1-ADAM22 from endocytosis-mediated degradation. If ADAM22 is not phosphorylated, then ADAM22 or the LGI1-ADAM22 heterodimer without 14-3-3 interactions is prone to endocytosis before forming the functional transsynaptic complex. This study also estimates the minimum amounts of ADAM22 and LGI1 proteins that can prevent seizure development. We suggest therapeutic options for human epilepsy to stabilize and increase the LGI1-ADAM22 complex by targeting PKA and 14-3-3.

Several questions still need to be clarified regarding the roles of the 14-3-3-ADAM22 interaction. First, does LGI1-ADAM22 heterodimer formation somehow involve 14-3-3 interactions? We showed that ADAM22^{SA}, lacking 14-3-3 interactions, retains binding to LGI1 in the *Adam22*$^{SA/SA}$ mouse brain (Figures 3C, 4A, and 4B), indicating that ADAM22 binds to LGI1 at the cell surface irrespective of 14-3-3 interactions. On the other hand, because immature and mature forms of ADAM22 are phosphorylated efficiently (Figure S1A), it is speculated that ADAM22 binds to 14-3-3 at the early stage of biogenesis like the CFTR protein (Liang et al., 2012) and then interacts with LGI1 on the cell surface. Given that 14-3-3 binding to phosphorylated CFTR facilitates its forward transport, further sensitive analysis will clarify whether 14-3-3 promotes ADAM22 trafficking to the cell surface and/or allosterically enhances the LGI1-ADAM22 interaction. Second, does 14-3-3 binding regulate the interaction of ADAM22 and PSD-95 at the synapse? We showed that 14-3-3 proteins and PSD-95 bind independently to ADAM22 and that a substantial portion

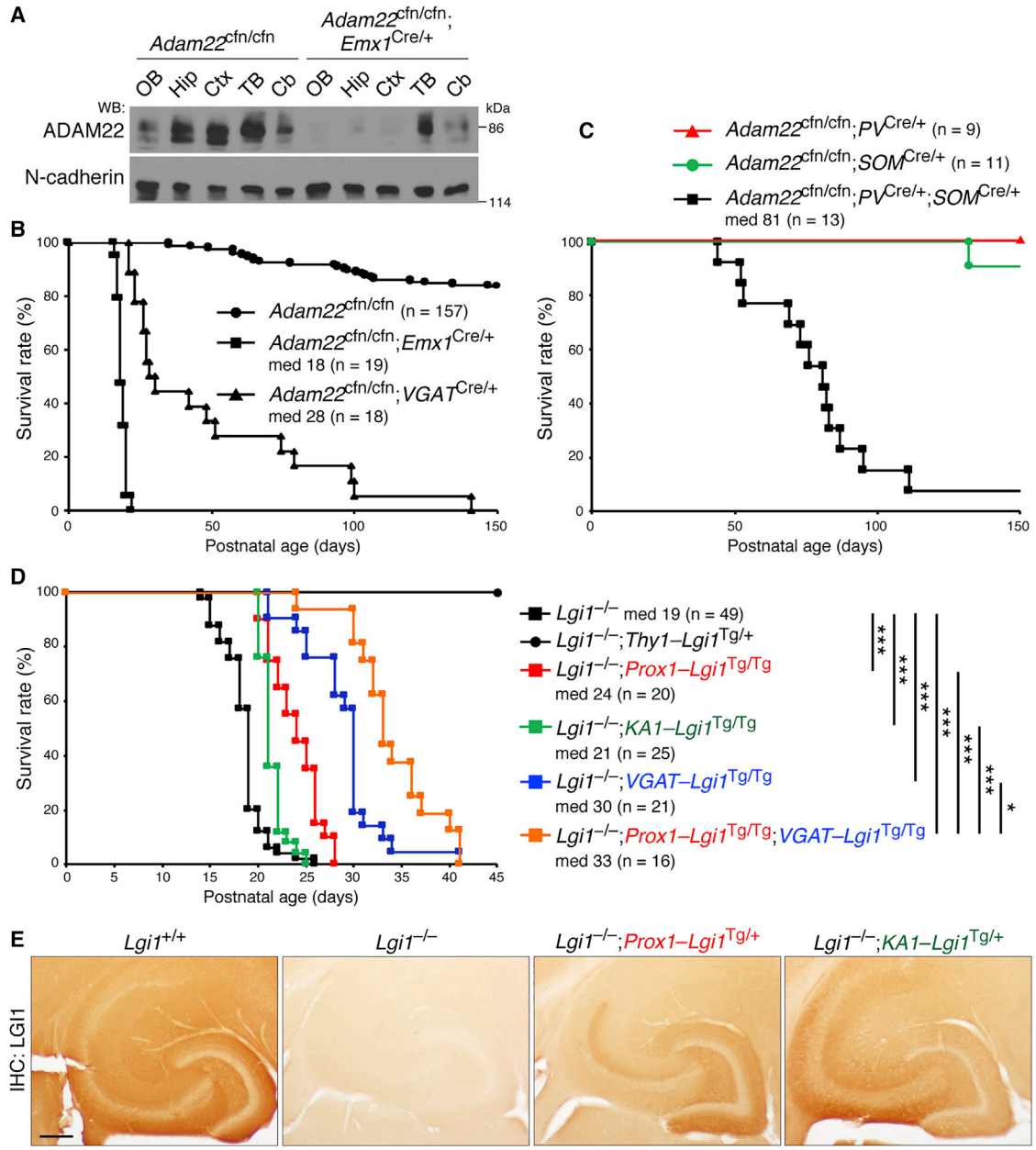

Figure 7. ADAM22 and LGI1 functions in excitatory and inhibitory neurons are essential for seizure suppression

(A) Reduced expression levels of ADAM22 in the forebrain of the *Adam22*$^{cfn/cfn}$;*Emx1*$^{Cre/+}$ mouse. OB, olfactory bulb; Hip, hippocampus; Ctx, cortex; TB, thalamus and brainstem; Cb, cerebellum.

(B and C) Kaplan-Meier survival plots of *Adam22*$^{cfn/cfn}$;*Emx1*$^{Cre/+}$ and *Adam22*$^{cfn/cfn}$;*VGAT*$^{Cre/+}$ mice (B) and of *Adam22*$^{cfn/cfn}$;*PV*$^{Cre/+}$, *Adam22*$^{cfn/cfn}$;*SOM*$^{Cre/+}$, and *Adam22*$^{cfn/cfn}$;*PV*$^{Cre/+}$;*SOM*$^{Cre/+}$ mice (C).

(D and E) Kaplan-Meier survival plots of different *Lgi1*$^{-/-}$ mice expressing the WT *Lgi1* transgene under the control of *Prox1*, *KA1*, or/and *VGAT* promoters (D). A log rank test was used for curve comparisons. *$p < 0.05$, ***$p < 0.001$. Dentate granule cell-specific and CA3 pyramidal neuron-specific expression of LGI1 are confirmed by immunohistochemistry with an anti-LGI1 antibody in *Lgi1*$^{-/-}$;*Prox1-Lgi1*$^{Tg/+}$ and *Lgi1*$^{-/-}$;*KA1-Lgi1*$^{Tg/+}$ mice, respectively (E). Scale bar, 200 μm.

See also Figures S7 and S8.

of LGI1-ADAM22-14-3-3 complexes contain PSD-95 in the brain (Figure S3). Although ADAM22 binds to PSD-95 in the absence of 14-3-3 interaction in *Adam22*$^{SA/SA}$ mice (Figures 4B), it is still an open question whether 14-3-3 binding reinforces the ADAM22-PSD-95 interaction to form and stabilize the functional transsynaptic protein complex. Third, does the accelerated endocytosis and subsequent lysosomal degradation of ADAM22 in the absence of 14-3-3 binding occur in neuronal compartments other than excitatory synapses? ADAM22 in the AIS of inhibitory cortical neurons was not

reduced in cultured neurons from the *Adam22*$^{SA/SA}$ mouse, whereas synaptic ADAM22 was reduced greatly (Figures 2F, 2G, and S2B–S2D). This result suggests another stabilization mechanism for ADAM22 in the AIS of inhibitory neurons. Further studies are required to understand subcellular compartment-specific mechanisms for ADAM22 degradation.

Stabilization of the 14-3-3-ADAM22 interaction could offer a therapeutic approach for epilepsy. Fusicoccin-A, a fungal toxin, is a small-molecule stabilizer of 14-3-3-client complexes by binding to a pocket created by the interface of the client motif and the 14-3-3 groove. Given the structure of 14-3-3 in complex with dually phosphorylated CFTR and fusicoccin-A (PDB: 5D3F; Stevers et al., 2016), it is speculated that 14-3-3 and the pS855 motif of ADAM22 could make a hydrophobic pocket to accommodate fusicoccin-A (Figures S5D and S5E). Although we could not observe the increased binding affinity of the ppADAM22 peptide to 14-3-3 in the presence of fusicoccin-A by ITC measurement (K_d values, 25.5 nM versus 90.1 nM), the effect of fusicoccin-A might be occluded because of the high-affinity binding between 14-3-3 and ppADAM22. Nevertheless, it may be worthwhile to explore other 14-3-3 stabilizers to increase 14-3-3-ADAM22 interactions. ADAM22 phosphorylation could be an alternative drug target because dual phosphorylation of ADAM22 synergically enhances the ADAM22 binding to 14-3-3. Because PKA efficiently phosphorylated ADAM22-S832 and -S855 (Figures 1E and S1), and forskolin-mediated PKA activation increased ADAM22-14-3-3 binding in heterologous cells (Figure 4G), PKA activation has high potential to increase the levels of LGI1-ADAM22 complex in the brain. Candidates include adenyl cyclase activators (e.g., forskolin) and phosphodiesterase (PDE) inhibitors (e.g., rolipram), which increase intracellular cAMP levels. PDE inhibitors especially attract much attention because they have been proposed for treatment of a broad spectrum of neuronal diseases, such as stroke, Alzheimer's disease, schizophrenia, and multiple sclerosis (Blokland et al., 2019). Future studies will be needed to demonstrate this possibility for epilepsy.

Understanding how much protein function is sufficient to protect from disease symptoms is an important future goal for disease treatment. If we obtained such quantitative information, then we would know how much LGI1-ADAM22 function needs to be restored and when we need to intervene. Using a series of hypomorphic mouse strains, we found that ~10% of ADAM22 and ~50% of LGI1 residual levels could suppress lethal spontaneous seizures in mice. Although these results are consistent with the inheritance patterns of LGI1-related familial epilepsy (autosomal dominant pattern) and ADAM22-related encephalopathy (autosomal recessive pattern) in humans, one may ask why LGI1 and ADAM22, which are in the same protein complex, display different dosage sensitivities. For efficient assembly of LGI1 and ADAM22, especially their transsynaptic supercomplexes, their local concentrations need to be balanced precisely. Therefore, the different dosage sensitivities could be explained by possible differences in some factors: (1) individual local concentrations of LGI1 and ADAM22 at the cell surface; (2) degrees of compensational or redundant expressions of their family proteins LGI2, LGI3, LGI4, and ADAM23 and ADAM11 (Fukata et al., 2010; Kegel et al., 2014); and (3) the spatiotemporal and cell-type expression patterns of LGI1 and ADAM22. Because excitatory/inhibitory (E/I) balance is regulated precisely in a circuit-specific manner in the brain, differential expression of LGI1 and ADAM22 across neural circuits could affect the degree of E/I imbalance when either of them is reduced. Further studies will be required to address the critical determinant of dosage sensitivity.

This study finds an essential role of LGI1 and ADAM22 in excitatory and inhibitory neurons (Figure 7). One may wonder how ADAM22 dysfunction in functionally opposite neuron types causes similar lethal epilepsy and whether LGI1-ADAM22 complexes have distinct functions in excitatory and inhibitory neurons to regulate neuronal excitability. LGI1-ADAM22 occurs at the excitatory synapses and directly regulates PSD-95-family MAGUK function, which anchor an array of membrane proteins, including α-amino-3-hydroxy-5-methyl-4-isoxazole-propionic acid (AMPA) receptor and Kv_1 channel (Fukata et al., 2006, 2021). Then, dysfunction of LGI1-ADAM22 causes reduced synaptic AMPA receptor function (Fukata et al., 2010; Lovero et al., 2015) and reduced axonal Kv_1 channel function (Seagar et al., 2017). This scenario suggests neuron-type-dependent pathogenic mechanisms: (1) reduced AMPA receptor function at the excitatory synapses of inhibitory neurons could cause disinhibition of overall neural network activity, and (2) reduced axonal Kv_1 channel function of principal excitatory neurons could increase intrinsic neuronal excitability. The combined dysfunctions could break the E/I balance and cause seizure activity in the neural network.

It has been reported that a reduction in AMPA receptor-mediated synaptic transmission could occur as a homeostatic consequence of an epileptic episode (Karmarkar and Buonomano, 2006; Müller et al., 1993; Turrigiano and Nelson, 2004). Thus, it may be controversial whether the reduced AMPA receptor-mediated synaptic transmission observed in epileptic *Lgi1* KO mice (Fukata et al., 2010) is a primary LoF effect for *Lgi1* or a secondary effect induced by repeated seizures. However, when AMPA receptor-mediated excitatory postsynaptic currents (EPSCs) are recorded from hippocampal slices, prepared from *Lgi1* KO mice at younger ages and before onset of observable seizures, reduced AMPA receptor currents are still observed (Lovero et al., 2015). Furthermore, AMPA receptor-mediated EPSCs are reduced greatly in Cre-transfected (*Adam22* KO) CA1 neurons compared with simultaneously recorded, neighboring, non-transfected neurons in cultured hippocampal slices from seizure-free *Adam22* floxed mice (Lovero et al., 2015). These results suggest that reduced excitatory synaptic transmission in LGI1- and ADAM22-deficient neurons is not necessarily caused by repeated seizures but represents their primary, LoF effect. Therefore, the reduced AMPA receptor function observed in *Lgi1* KO mice may involve two non-mutually exclusive effects: (1) a primary dysfunction of transsynaptic LGI1-ADAM22-MAGUK (Fukata et al., 2021) and (2) a secondary, homeostatic consequence of an epileptic activity.

Currently used anti-epileptic drugs mainly modulate GABAergic (e.g., diazepam), glutamatergic (e.g., perampanel), or voltage-dependent sodium/potassium (e.g., carbamazepine) channel properties, sometimes causing serious adverse effects in the central nervous system, such as sedation,

dizziness, and cognitive deficits. Reinforcement of the LGI1-ADAM22 pathway could be a better alternative to minimize side effects because it finely regulates glutamate receptor function and potassium channel function and normalizes the overall E/I balance in the neuronal network. We suggest that the biogenesis pathway of ADAM22, involving PKA and 14-3-3 proteins, could be a promising drug target for neurological disorders such as epilepsy.

Limitations of the study

This study reveals that dual phosphorylation of ADAM22 mediates its stable interaction with 14-3-3. However, how much Ser855 phosphorylation contributes to the ADAM22-14-3-3 interaction remains unclear because the stoichiometry of ADAM22-Ser855 phosphorylation in the brain is elusive. Given a small but quantitative migration shift of ADAM22^{S832A} in the Phos-tag gel in the *Adam22*$^{S832A/S832A}$ mouse brain (Figure 2A, white arrowhead), a substantial amount of ADAM22 may be phosphorylated at residues besides Ser832. An intriguing possibility is that phosphorylation levels of Ser855, unlike stably phosphorylated Ser832, could be regulated upon synaptic activity, allowing dynamic regulation of the ADAM22-14-3-3 interaction. The study also estimates the minimal amounts of ADAM22 and LGI1 proteins that can prevent seizure phenotypes. However, this estimation was done using mouse forebrain lysates, and therefore spatiotemporal information is missing. Nevertheless, our study will serve as a prototype for molecular precision medicine and has strong translational potential for LoF genetic disorders.

STAR★METHODS

Detailed methods are provided in the online version of this paper and include the following:

- KEY RESOURCES TABLE
- RESOURCE AVAILABILITY
  - Lead contact
  - Materials availability
  - Data and code availability
- EXPERIMENTAL MODEL AND SUBJECT DETAILS
  - Mice
  - Rat or mouse primary neuronal culture
  - Cell lines
- METHOD DETAILS
  - Cloning and plasmid constructions
  - Generation of *Adam22*^{S832A} knock-in mouse
  - Generation of conditional *Adam22* knockout mice
  - Generation of transgenic mice for cell-type specific LGI1 expression
  - Induction and scoring of seizures
  - Biochemical analysis of brain lysates
  - Endo H and PNGase F treatment
  - Phos-tag SDS-PAGE
  - Immunoprecipitation from the mouse brain
  - Reprecipitation of PSD-95 from ADAM22-containing complexes
  - Determination of ADAM22 phosphorylation sites
  - *In vitro* phosphorylation assay
  - Blue-Native PAGE
  - Purification from heterologous cells
  - Cell-surface biotinylation assay
  - Quantitative western blotting
  - Immunohistochemistry
  - Immunofluorescence analysis of cultured neurons
  - ITC
  - Crystallography of 14-3-3ζ–ppADAM22 complex
- QUANTIFICATION AND STATISTICAL ANALYSIS

SUPPLEMENTAL INFORMATION

Supplemental information can be found online at https://doi.org/10.1016/j.celrep.2021.110107.

ACKNOWLEDGMENTS

We thank Yumiko Makino (Functional Genomics Facility, NIBB Core Research Facilities) for LC-MS/MS analysis, Yumi Suzuki (NIPS) for technical assistance, and Dr. Teruyuki Tanaka (The University of Tokyo) and Dr. Ulli Bayer (University of Colorado) for providing plasmid vectors. This work was supported by grants from the Ministry of Education Culture, Sports, Science and Technology (19K06893 to N.Y.; 19H03331 and 19K22439 to Y.F.; 19H03162 to A.Y.; 19K16269 to Y.M.; 18H03983 to S.F.; and 19K22548, 20H04915, and 20H00459 to M.F.), the Japan Agency for Medical Research and Development (21wm0525022h0001 to Y.F.), and the Takeda Science Foundation (to M.F.).

AUTHOR CONTRIBUTIONS

N.Y., Y.F., S.F., and M.F. designed the research. N.Y. performed the mouse experiments. N.Y. and Y.F. performed biochemistry experiments. N.Y., Y.F., M.S., T.G., M.H., and M.F. generated knockin and transgenic mice. K.O., A.Y., Y.L., and S.F. performed structural analyses. Y.M., M.A., H.K., K.S., and D.M. prepared critical mouse resources. N.Y., Y.F., S.F., and M.F. drafted the manuscript, and all authors revised or commented on it.

DECLARATION OF INTERESTS

The authors declare no competing interests.

Received: July 19, 2021
Revised: October 8, 2021
Accepted: November 16, 2021
Published: December 14, 2021

REFERENCES

Blokland, A., Heckman, P., Vanmierlo, T., Schreiber, R., Paes, D., and Prickaerts, J. (2019). Phosphodiesterase Type 4 Inhibition in CNS Diseases. Trends Pharmacol. Sci. *40*, 971–985.

Boillot, M., Huneau, C., Marsan, E., Lehongre, K., Navarro, V., Ishida, S., Dufresnois, B., Ozkaynak, E., Garrigue, J., Miles, R., et al. (2014). Glutamatergic neuron-targeted loss of LGI1 epilepsy gene results in seizures. Brain *137*, 2984–2996.

Bonetto, G., Hivert, B., Goutebroze, L., Karagogeos, D., Crépel, V., and Faivre-Sarrailh, C. (2019). Selective Axonal Expression of the Kv1 Channel Complex in Pre-myelinated GABAergic Hippocampal Neurons. Front. Cell. Neurosci. *13*, 222.

Bridges, D., and Moorhead, G.B. (2005). 14-3-3 proteins: a number of functions for a numbered protein. Sci. STKE *2005*, re10.

Chabrol, E., Navarro, V., Provenzano, G., Cohen, I., Dinocourt, C., Rivaud-Péchoux, S., Fricker, D., Baulac, M., Miles, R., Leguern, E., and Baulac, S. (2010). Electroclinical characterization of epileptic seizures in leucine-rich, glioma-inactivated 1-deficient mice. Brain *133*, 2749–2762.

Chen, X., Fukata, Y., Fukata, M., and Nicoll, R.A. (2021). MAGUKs are essential, but redundant, in long-term potentiation. Proc. Natl. Acad. Sci. USA *118*, e2107585118.

Emsley, P., Lohkamp, B., Scott, W.G., and Cowtan, K. (2010). Features and development of Coot. Acta Crystallogr. D Biol. Crystallogr. *66*, 486–501.

Frank, R.A., Komiyama, N.H., Ryan, T.J., Zhu, F., O'Dell, T.J., and Grant, S.G. (2016). NMDA receptors are selectively partitioned into complexes and supercomplexes during synapse maturation. Nat. Commun. *7*, 11264.

Fukata, Y., Adesnik, H., Iwanaga, T., Bredt, D.S., Nicoll, R.A., and Fukata, M. (2006). Epilepsy-related ligand/receptor complex LGI1 and ADAM22 regulate synaptic transmission. Science *313*, 1792–1795.

Fukata, Y., Lovero, K.L., Iwanaga, T., Watanabe, A., Yokoi, N., Tabuchi, K., Shigemoto, R., Nicoll, R.A., and Fukata, M. (2010). Disruption of LGI1-linked synaptic complex causes abnormal synaptic transmission and epilepsy. Proc. Natl. Acad. Sci. USA *107*, 3799–3804.

Fukata, Y., Chen, X., Chiken, S., Hirano, Y., Yamagata, A., Inahashi, H., Sanbo, M., Sano, H., Goto, T., Hirabayashi, M., et al. (2021). LGI1-ADAM22-MAGUK configures transsynaptic nanoalignment for synaptic transmission and epilepsy prevention. Proc. Natl. Acad. Sci. USA *118*, e2022580118.

Gödde, N.J., D'Abaco, G.M., Paradiso, L., and Novak, U. (2006). Efficient ADAM22 surface expression is mediated by phosphorylation-dependent interaction with 14-3-3 protein family members. J. Cell Sci. *119*, 3296–3305.

Gödde, N.J., D'Abaco, G.M., Paradiso, L., and Novak, U. (2007). Differential coding potential of ADAM22 mRNAs. Gene *403*, 80–88.

Gu, W., Brodtkorb, E., and Steinlein, O.K. (2002). LGI1 is mutated in familial temporal lobe epilepsy characterized by aphasic seizures. Ann. Neurol. *52*, 364–367.

Irani, S.R., Alexander, S., Waters, P., Kleopa, K.A., Pettingill, P., Zuliani, L., Peles, E., Buckley, C., Lang, B., and Vincent, A. (2010). Antibodies to Kv1 potassium channel-complex proteins leucine-rich, glioma inactivated 1 protein and contactin-associated protein-2 in limbic encephalitis, Morvan's syndrome and acquired neuromyotonia. Brain *133*, 2734–2748.

Kabsch, W. (2010). Xds. Acta Crystallogr. D Biol. Crystallogr. *66*, 125–132.

Kalachikov, S., Evgrafov, O., Ross, B., Winawer, M., Barker-Cummings, C., Martinelli Boneschi, F., Choi, C., Morozov, P., Das, K., Teplitskaya, E., et al. (2002). Mutations in LGI1 cause autosomal-dominant partial epilepsy with auditory features. Nat. Genet. *30*, 335–341.

Karmarkar, U.R., and Buonomano, D.V. (2006). Different forms of homeostatic plasticity are engaged with distinct temporal profiles. Eur. J. Neurosci. *23*, 1575–1584.

Kassai, H., Terashima, T., Fukaya, M., Nakao, K., Sakahara, M., Watanabe, M., and Aiba, A. (2008). Rac1 in cortical projection neurons is selectively required for midline crossing of commissural axonal formation. Eur. J. Neurosci. *28*, 257–267.

Kast, D.J., and Dominguez, R. (2019). Mechanism of IRSp53 inhibition by 14-3-3. Nat. Commun. *10*, 483.

Kegel, L., Jaegle, M., Driegen, S., Aunin, E., Leslie, K., Fukata, Y., Watanabe, M., Fukata, M., and Meijer, D. (2014). Functional phylogenetic analysis of LGI proteins identifies an interaction motif crucial for myelination. Development *141*, 1749–1756.

Kinoshita, E., Kinoshita-Kikuta, E., and Koike, T. (2009). Separation and detection of large phosphoproteins using Phos-tag SDS-PAGE. Nat. Protoc. *4*, 1513–1521.

Kono, J., Konno, K., Talukder, A.H., Fuse, T., Abe, M., Uchida, K., Horio, S., Sakimura, K., Watanabe, M., and Itoi, K. (2017). Distribution of corticotropin-releasing factor neurons in the mouse brain: a study using corticotropin-releasing factor-modified yellow fluorescent protein knock-in mouse. Brain Struct. Funct. *222*, 1705–1732.

Kornau, H.C., Kreye, J., Stumpf, A., Fukata, Y., Parthier, D., Sammons, R.P., Imbrosci, B., Kurpjuweit, S., Kowski, A.B., Fukata, M., et al. (2020). Human Cerebrospinal Fluid Monoclonal LGI1 Autoantibodies Increase Neuronal Excitability. Ann. Neurol. *87*, 405–418.

Kostelecky, B., Saurin, A.T., Purkiss, A., Parker, P.J., and McDonald, N.Q. (2009). Recognition of an intra-chain tandem 14-3-3 binding site within PKCepsilon. EMBO Rep. *10*, 983–989.

Lai, M., Huijbers, M.G., Lancaster, E., Graus, F., Bataller, L., Balice-Gordon, R., Cowell, J.K., and Dalmau, J. (2010). Investigation of LGI1 as the antigen in limbic encephalitis previously attributed to potassium channels: a case series. Lancet Neurol. *9*, 776–785.

Liang, X., Da Paula, A.C., Bozoky, Z., Zhang, H., Bertrand, C.A., Peters, K.W., Forman-Kay, J.D., and Frizzell, R.A. (2012). Phosphorylation-dependent 14-3-3 protein interactions regulate CFTR biogenesis. Mol. Biol. Cell *23*, 996–1009.

Liebschner, D., Afonine, P.V., Baker, M.L., Bunkóczi, G., Chen, V.B., Croll, T.I., Hintze, B., Hung, L.W., Jain, S., McCoy, A.J., et al. (2019). Macromolecular structure determination using X-rays, neutrons and electrons: recent developments in Phenix. Acta Crystallogr. D Struct. Biol. *75*, 861–877.

Lovero, K.L., Fukata, Y., Granger, A.J., Fukata, M., and Nicoll, R.A. (2015). The LGI1-ADAM22 protein complex directs synapse maturation through regulation of PSD-95 function. Proc. Natl. Acad. Sci. USA *112*, E4129–E4137.

Lugarà, E., Kaushik, R., Leite, M., Chabrol, E., Dityatev, A., Lignani, G., and Walker, M.C. (2020). LGI1 downregulation increases neuronal circuit excitability. Epilepsia *61*, 2836–2846.

Maddirevula, S., Alzahrani, F., Al-Owain, M., Al Muhaizea, M.A., Kayyali, H.R., AlHashem, A., Rahbeeni, Z., Al-Otaibi, M., Alzaidan, H.I., Balobaid, A., et al. (2019). Autozygome and high throughput confirmation of disease genes candidacy. Genet. Med. *21*, 736–742.

Marsden, K.C., Shemesh, A., Bayer, K.U., and Carroll, R.C. (2010). Selective translocation of Ca2+/calmodulin protein kinase IIalpha (CaMKIIalpha) to inhibitory synapses. Proc. Natl. Acad. Sci. USA *107*, 20559–20564.

Molzan, M., and Ottmann, C. (2012). Synergistic binding of the phosphorylated S233- and S259-binding sites of C-RAF to one 14-3-3ζ dimer. J. Mol. Biol. *423*, 486–495.

Morante-Redolat, J.M., Gorostidi-Pagola, A., Piquer-Sirerol, S., Sáenz, A., Poza, J.J., Galán, J., Gesk, S., Sarafidou, T., Mautner, V.F., Binelli, S., et al. (2002). Mutations in the LGI1/Epitempin gene on 10q24 cause autosomal dominant lateral temporal epilepsy. Hum. Mol. Genet. *11*, 1119–1128.

Müller, M., Gähwiler, B.H., Rietschin, L., and Thompson, S.M. (1993). Reversible loss of dendritic spines and altered excitability after chronic epilepsy in hippocampal slice cultures. Proc. Natl. Acad. Sci. USA *90*, 257–261.

Muona, M., Fukata, Y., Anttonen, A.K., Laari, A., Palotie, A., Pihko, H., Lönnqvist, T., Valanne, L., Somer, M., Fukata, M., and Lehesjoki, A.E. (2016). Dysfunctional ADAM22 implicated in progressive encephalopathy with cortical atrophy and epilepsy. Neurol. Genet. *2*, e46.

Noebels, J. (2015). Pathway-driven discovery of epilepsy genes. Nat. Neurosci. *18*, 344–350.

Noritake, J., Fukata, Y., Iwanaga, T., Hosomi, N., Tsutsumi, R., Matsuda, N., Tani, H., Iwanari, H., Mochizuki, Y., Kodama, T., et al. (2009). Mobile DHHC palmitoylating enzyme mediates activity-sensitive synaptic targeting of PSD-95. J. Cell Biol. *186*, 147–160.

Ohkawa, T., Fukata, Y., Yamasaki, M., Miyazaki, T., Yokoi, N., Takashima, H., Watanabe, M., Watanabe, O., and Fukata, M. (2013). Autoantibodies to epilepsy-related LGI1 in limbic encephalitis neutralize LGI1-ADAM22 interaction and reduce synaptic AMPA receptors. J. Neurosci. *33*, 18161–18174.

Ozkaynak, E., Abello, G., Jaegle, M., van Berge, L., Hamer, D., Kegel, L., Driegen, S., Sagane, K., Bermingham, J.R., Jr., and Meijer, D. (2010). Adam22 is a major neuronal receptor for Lgi4-mediated Schwann cell signaling. J. Neurosci. *30*, 3857–3864.

Petit-Pedrol, M., Sell, J., Planagumà, J., Mannara, F., Radosevic, M., Haselmann, H., Ceanga, M., Sabater, L., Spatola, M., Soto, D., et al. (2018). LGI1 antibodies alter Kv1.1 and AMPA receptors changing synaptic excitability, plasticity and memory. Brain *141*, 3144–3159.

Ramberger, M., Berretta, A., Tan, J.M.M., Sun, B., Michael, S., Yeo, T., Theorell, J., Bashford-Rogers, R., Paneva, S., O'Dowd, V., et al. (2020). Distinctive binding properties of human monoclonal LGI1 autoantibodies determine pathogenic mechanisms. Brain *143*, 1731–1745.

Rivers, A., Gietzen, K.F., Vielhaber, E., and Virshup, D.M. (1998). Regulation of casein kinase I epsilon and casein kinase I delta by an in vivo futile phosphorylation cycle. J. Biol. Chem. *273*, 15980–15984.

Sagane, K., Hayakawa, K., Kai, J., Hirohashi, T., Takahashi, E., Miyamoto, N., Ino, M., Oki, T., Yamazaki, K., and Nagasu, T. (2005). Ataxia and peripheral nerve hypomyelination in ADAM22-deficient mice. BMC Neurosci. *6*, 33.

Schägger, H. (2001). Blue-native gels to isolate protein complexes from mitochondria. Methods Cell Biol. *65*, 231–244.

Seagar, M., Russier, M., Caillard, O., Maulet, Y., Fronzaroli-Molinieres, L., De San Feliciano, M., Boumedine-Guignon, N., Rodriguez, L., Zbili, M., Usseglio, F., et al. (2017). LGI1 tunes intrinsic excitability by regulating the density of axonal Kv1 channels. Proc. Natl. Acad. Sci. USA *114*, 7719–7724.

Smith, A.J., Daut, J., and Schwappach, B. (2011). Membrane proteins as 14-3-3 clients in functional regulation and intracellular transport. Physiology (Bethesda) *26*, 181–191.

Soh, J.W., and Weinstein, I.B. (2003). Roles of specific isoforms of protein kinase C in the transcriptional control of cyclin D1 and related genes. J. Biol. Chem. *278*, 34709–34716.

Stambolic, V., and Woodgett, J.R. (1994). Mitogen inactivation of glycogen synthase kinase-3 beta in intact cells via serine 9 phosphorylation. Biochem. J. *303*, 701–704.

Steinlein, O.K. (2004). Genetic mechanisms that underlie epilepsy. Nat. Rev. Neurosci. *5*, 400–408.

Stevers, L.M., Lam, C.V., Leysen, S.F., Meijer, F.A., van Scheppingen, D.S., de Vries, R.M., Carlile, G.W., Milroy, L.G., Thomas, D.Y., Brunsveld, L., and Ottmann, C. (2016). Characterization and small-molecule stabilization of the multisite tandem binding between 14-3-3 and the R domain of CFTR. Proc. Natl. Acad. Sci. USA *113*, E1152–E1161.

Tokumasu, R., Yamaga, K., Yamazaki, Y., Murota, H., Suzuki, K., Tamura, A., Bando, K., Furuta, Y., Katayama, I., and Tsukita, S. (2016). Dose-dependent role of claudin-1 in vivo in orchestrating features of atopic dermatitis. Proc. Natl. Acad. Sci. USA *113*, E4061–E4068.

Tremblay, R., Lee, S., and Rudy, B. (2016). GABAergic Interneurons in the Neocortex: From Cellular Properties to Circuits. Neuron *91*, 260–292.

Turowec, J.P., Duncan, J.S., French, A.C., Gyenis, L., St Denis, N.A., Vilk, G., and Litchfield, D.W. (2010). Protein kinase CK2 is a constitutively active enzyme that promotes cell survival: strategies to identify CK2 substrates and manipulate its activity in mammalian cells. Methods Enzymol. *484*, 471–493.

Turrigiano, G.G., and Nelson, S.B. (2004). Homeostatic plasticity in the developing nervous system. Nat. Rev. Neurosci. *5*, 97–107.

Vagin, A., and Teplyakov, A. (1997). MOLREP: an automated program for molecular replacement. J. Appl. Cryst. *30*, 1022–1025.

Watton, S.J., and Downward, J. (1999). Akt/PKB localisation and 3′ phosphoinositide generation at sites of epithelial cell-matrix and cell-cell interaction. Curr. Biol. *9*, 433–436.

Winn, M.D., Ballard, C.C., Cowtan, K.D., Dodson, E.J., Emsley, P., Evans, P.R., Keegan, R.M., Krissinel, E.B., Leslie, A.G., McCoy, A., et al. (2011). Overview of the CCP4 suite and current developments. Acta Crystallogr. D Biol. Crystallogr. *67*, 235–242.

Wittig, I., Braun, H.P., and Schägger, H. (2006). Blue native PAGE. Nat. Protoc. *1*, 418–428.

Yaffe, M.B., Rittinger, K., Volinia, S., Caron, P.R., Aitken, A., Leffers, H., Gamblin, S.J., Smerdon, S.J., and Cantley, L.C. (1997). The structural basis for 14-3-3:phosphopeptide binding specificity. Cell *91*, 961–971.

Yamagata, A., Miyazaki, Y., Yokoi, N., Shigematsu, H., Sato, Y., Goto-Ito, S., Maeda, A., Goto, T., Sanbo, M., Hirabayashi, M., et al. (2018). Structural basis of epilepsy-related ligand-receptor complex LGI1-ADAM22. Nat. Commun. *9*, 1546.

Yokoi, N., Fukata, Y., Kase, D., Miyazaki, T., Jaegle, M., Ohkawa, T., Takahashi, N., Iwanari, H., Mochizuki, Y., Hamakubo, T., et al. (2015). Chemical corrector treatment ameliorates increased seizure susceptibility in a mouse model of familial epilepsy. Nat. Med. *21*, 19–26.

Young, N.P., Kamireddy, A., Van Nostrand, J.L., Eichner, L.J., Shokhirev, M.N., Dayn, Y., and Shaw, R.J. (2016). AMPK governs lineage specification through Tfeb-dependent regulation of lysosomes. Genes Dev. *30*, 535–552.

Yu, Y.E., Wen, L., Silva, J., Li, Z., Head, K., Sossey-Alaoui, K., Pao, A., Mei, L., and Cowell, J.K. (2010). Lgi1 null mutant mice exhibit myoclonic seizures and CA1 neuronal hyperexcitability. Hum. Mol. Genet. *19*, 1702–1711.

Zhong, H., Sia, G.M., Sato, T.R., Gray, N.W., Mao, T., Khuchua, Z., Huganir, R.L., and Svoboda, K. (2009). Subcellular dynamics of type II PKA in neurons. Neuron *62*, 363–374.

Zhou, L., Hossain, M.I., Yamazaki, M., Abe, M., Natsume, R., Konno, K., Kageyama, S., Komatsu, M., Watanabe, M., Sakimura, K., and Takebayashi, H. (2018a). Deletion of exons encoding carboxypeptidase domain of Nna1 results in Purkinje cell degeneration (pcd) phenotype. J. Neurochem. *147*, 557–572.

Zhou, L., Zhou, L., Su, L.D., Cao, S.L., Xie, Y.J., Wang, N., Shao, C.Y., Wang, Y.N., Zhou, J.H., Cowell, J.K., and Shen, Y. (2018b). Celecoxib Ameliorates Seizure Susceptibility in Autosomal Dominant Lateral Temporal Epilepsy. J. Neurosci. *38*, 3346–3357.

Zhu, P.c., Sun, Y., Xu, R., Sang, Y., Zhao, J., Liu, G., Cai, L., Li, C., and Zhao, S. (2003). The interaction between ADAM 22 and 14-3-3zeta: regulation of cell adhesion and spreading. Biochem. Biophys. Res. Commun. *301*, 991–999.

STAR★METHODS

KEY RESOURCES TABLE

REAGENT or RESOURCE	SOURCE	IDENTIFIER
Antibodies		
Rabbit polyclonal anti-ADAM22 (R2)	Fukata et al., 2010	N/A
Rabbit polyclonal anti-ADAM22 (R4)	This paper	N/A
Rabbit polyclonal anti-ADAM23	Abcam	Cat#ab28302; RRID: AB_722575
Rabbit polyclonal anti-FAH tag (GGDYKDDDDKGGDTYR YIGGYPYDVPDYAGG)	Lovero et al., 2015	N/A
Rabbit polyclonal anti-FH tag (DYKDDDD KGGHHHHHH)	Yokoi et al., 2015	N/A
Rabbit polyclonal anti-$GABA_A$ receptor β3	Abcam	Cat#ab4046; RRID: AB_2109564
Rabbit polyclonal anti-His tag	MBL	Cat#PM032; RRID: AB_843163
Rabbit polyclonal anti-LGI1	Abcam	Cat#ab30868, lot 223017, this lot is not available now; RRID: AB_776017
Rabbit polyclonal anti-phospho-ADAM22 Ser832 (mouse, aa 827-836; RPRSN***pS***WQGN)	This paper	N/A
Rabbit polyclonal anti-PSD-95	Noritake et al., 2009	N/A
Mouse monoclonal anti-α-Adaptin (Clone 8/Adaptin α)	BD Biosciences	Cat#610501; RRID: AB_2313949
Mouse monoclonal anti-Actin (Clone C4)	Merck Millipore	Cat#MAB1501; RRID: AB_2223041
Mouse monoclonal anti-ADAM22 (Clone N46/30)	NeuroMab	Cat#75-083; RRID: AB_10675128
Mouse monoclonal anti-β-Catenin (Clone 14/Beta-Catenin)	BD Biosciences	Cat#610153; RRID: AB_397554
Mouse monoclonal anti-CaMKIIα (Clone 6G9)	Merck Millipore	Cat#05-532; RRID: AB_2314080
Mouse monoclonal anti-GAD67 (Clone 1G10.2)	Sigma-Aldrich	Cat#MAB5406; RRID: AB_2278725
Mouse monoclonal anti-GFP (Clone 1E4)	MBL	Cat#M048-3; RRID: AB_591823
Mouse monoclonal anti-HA (Clone 16B2)	Covance	Cat#MMS-101P; RRID: AB_10064068
Mouse monoclonal anti-Kv1.2α (Clone K14/16)	NeuroMab	Cat#75-008; RRID: AB_2296313
Mouse monoclonal anti-Kv4.2 (Clone K57/1)	NeuroMab	Cat#75-016; RRID: AB_2131945
Mouse monoclonal anti-N-Cadherin (Clone 32/N-Cadherin)	BD Biosciences	Cat#610920; RRID: AB_2077527
Mouse monoclonal anti-pan 14-3-3 (Clone H-8)	Santa Cruz	Cat#sc-1657; RRID:AB_626618
Mouse monoclonal anti-Parvalbumin (Clone PARV-19)	Sigma-Aldrich	Cat#P3088; RRID: AB_477329
Mouse monoclonal anti-PSD-95 (Clone 7E3-1B8)	Thermo Fisher Scientific	Cat#MA1-046; RRID: AB_2092361
Rat monoclonal anti-Somatostatin (Clone YC7)	Merck Millipore	Cat#MAB354; RRID: AB_2255365
Guinea pig polyclonal anti-Ankyrin-G	Synaptic Systems	Cat#386005; RRID: AB_2737033
Guinea pig polyclonal anti-LGI1	Yokoi et al., 2015	N/A

(*Continued on next page*)

Continued

REAGENT or RESOURCE	SOURCE	IDENTIFIER
Bacterial and virus strains		
Escherichia coli DH5α cells	Takara Bio	Cat#9057
Escherichia coli Rosetta (DE3)	Merck Millipore	Cat#70954
Chemicals, peptides, and recombinant proteins		
Pentylenetetrazole	Sigma-Aldrich	Cat#P6500
Cycloheximide	Sigma-Aldrich	Cat#C1988
Protein kinase A Catalytic Subunit from bovine heart	Sigma-Aldrich	Cat#P2645
MG-132	Merck Millipore	Cat#474790
Leupeptin Hemisulfate Monohydrate	WAKO	Cat#128-03753
Chloroquine Diphosphate	WAKO	Cat#036-13972
Forskolin	Alomone	Cat#F-500
Fusicoccin	Enzo	Cat#BML-E13340001
Endoglycosidase H	New England Biolabs	Cat#P0702
Peptide-N-Glycosidase F	New England Biolabs	Cat#P0704
Lambda Protein Phosphatase	New England Biolabs	Cat#P0753
TALON Affinity Resin	Clontech	Cat#635501
Pierce High Capacity NeutrAvidin Agarose	Thermo Fisher Scientific	Cat#29202
EZ-Link Sulfo-NHS-SS-Biotin	Thermo Fisher Scientific	Cat#29331
Protein A Sepharose CL-4B	GE Healthcare	Cat#17078001
Anti-FLAG M2 affinity gel	Merck Millipore	Cat#A2220
FLAG peptide	Sigma-Aldrich	Cat#F3290
Phos-tag Acrylamide AAL-107	WAKO	Cat#304-93521
Blue-G	Serva	Cat#35050.01
NuPAGE transfer buffer	Thermo Fisher Scientific	Cat#NP0006
EzFastBlot HMW	ATTO	Cat#WSE-7200
WIDE-VIEW Prestained Protein Size Marker III	WAKO	Cat#230-02461
Pre-stained Protein Markers (Broad Range) for SDS-PAGE	nacalai tesque	Cat#02525-35
Protein Ladder One Plus, Triple-color for SDS-PAGE	nacalai tesque	Cat#19593-25
Power SYBR green PCR Master Mix	Applied Biosciences	Cat#4367659
Lipofectamine	Thermo Fisher Scientific	Cat#18324012
Plus reagent	Thermo Fisher Scientific	Cat#11514015
Rat Nucleofector kit	Lonza	Cat#LZ-VPG-1003
Pepsin	Dako	Cat#S3002
Papain	Worthington	Cat#LS003126
Sequencing Grade Modified Trypsin	Promega	Cat#V5113
DNase I from bovine pancreas Type IV	Sigma-Aldrich	Cat#D5025
B-27	Thermo Fisher Scientific	Cat#17504044
GlutaMax	Thermo Fisher Scientific	Cat#35050061
Horse serum, heat inactivated	Thermo Fisher Scientific	Cat#26050088
Fetal bovine serum	Sigma-Aldrich	Cat#172012
Polyethylenimine	Sigma-Aldrich	Cat#P3143
Rat tail Type I Collagen	Corning	Cat#354236
Poly-L-Lysine hydrobromide	Sigma-Aldrich	Cat#P6282
pADAM22 peptide (RPRSN**pS**WQGN)	Eurofins Genomics	N/A
ppADAM22 peptide (RPRSN**pS**WQGNMG GNKKKIRGKRFRPRSN**pS**TE)	SCRUM	N/A

(*Continued on next page*)

Continued

REAGENT or RESOURCE	SOURCE	IDENTIFIER
Critical commercial assays		
SuperScript III First-Strand Synthesis System	Thermo Fisher Scientific	Cat#18080051
Elite ABC-HRP Kit	Vector Laboratories	Cat#PK-6100
DAB substrate Kit	Vector Laboratories	Cat#SK-4100
Deposited data		
ppADAM22–14-3-3ζ structure	This paper	PDB: 7EXE
Experimental Models: cell lines		
COS7	ATCC	Cat#CRL-1651
HEK293T	ATCC	Cat#CRL-3216
Rat primary hippocampal neurons	N/A	N/A
Mouse primary cortical neurons	N/A	N/A
Experimental models: Organisms/strains		
Mouse: *Adam22* Ser832Ala knock-in	This paper	N/A
Mouse: *Adam22*-FAH knock-in	Fukata et al., 2021	N/A
Mouse: *Adam22* cfn	Ozkaynak et al., 2010	N/A
Mouse: *Adam22* flox	Ozkaynak et al., 2010	N/A
Mouse: *Lgi1* knockout	Fukata et al., 2010	N/A
Mouse: *Thy1–Lgi1-FH* transgenic	Fukata et al., 2010	N/A
Mouse: *Prox1–Lgi1-FH* transgenic	Lovero et al., 2015	N/A
Mouse: *KA1–Lgi1-FH* transgenic	This paper	N/A
Mouse: *VGAT–Lgi1-FH* transgenic	This paper	N/A
Mouse: *Actb–iCre*	Zhou et al., 2018a	N/A
Mouse: *Actb–FLPe*	Kono et al., 2017	N/A
Mouse: *Emx1–Cre*	Kassai et al., 2008	N/A
Mouse: *Slc32a1*$^{tm2(cre)Lowl}$/J (Vgat-ires-Cre)	The Jackson Laboratory	Cat#016962; RRID: IMSR_JAX:016962
Mouse: B6;129P2-*Pvalb*$^{tm1(cre)Arbr}$/J (PV-ires-Cre)	The Jackson Laboratory	Cat#008069; RRID: IMSR_JAX:008069
Mouse: *Sst*$^{tm2.1(cre)Zjh}$/J (SOM-ires-Cre)	The Jackson Laboratory	Cat#013044; RRID: IMSR_JAX:013044
Mouse: B57BL/6N	Japan SLC	N/A
Mouse: B6D2F1	Japan SLC	N/A
Oligonucleotides		
See Table S2 for oligonucleotide sequences	N/A	N/A
Recombinant DNA		
pX330: mouse ADAM22-exon28-gr#1 for *Adam22* Ser832Ala knock-in (for genome-editing)	This paper	N/A
pCAGGS: mouse ADAM22	Fukata et al., 2006	N/A
pCAGGS: mouse ADAM22 Ser832Ala	This paper	N/A
pCAGGS: mouse ADAM22 Ser855Ala	This paper	N/A
pCAGGS: mouse ADAM22 Ser860Ala	This paper	N/A
pCAGGS: mouse ADAM22 Ser864Ala	This paper	N/A
pCAGGS: mouse ADAM22 Ser832Ala/Ser855Ala	This paper	N/A
pCAGGS: mouse ADAM22 Ser832Ala/ Ser855Ala/Ser860Ala/Ser864Ala	This paper	N/A
pCAGGS: mouse ADAM22-FLAG (extracellular)	This paper	N/A

(*Continued on next page*)

Continued

REAGENT or RESOURCE	SOURCE	IDENTIFIER
pCAGGS: mouse ADAM22 Ser832Ala-FLAG (extracellular)	This paper	N/A
pCAGGS: mouse ADAM22 Tyr758Ala/ Tyr783Ala/Ser832Ala-FLAG (extracellular)	This paper	N/A
pGEX-4T-1: mouse ADAM22 (aa 802-904)	This paper	N/A
pEGFP-C1: human ADAM22 cytoplasmic region (aa 759-906)	This paper	N/A
pCAGGS: GFP	This paper	N/A
pCAGGS: His_{x6}-14-3-3ε	This paper	N/A
pCAGGS: His_{x6}-14-3-3ζ	This paper	N/A
pCAGGS: His_{x6}-14-3-3ζ Arg56Ala/Arg60Ala	This paper	N/A
pCold I: His_{x6}-14-3-3ε	This paper	N/A
pCold I: His_{x6}-14-3-3ζ	This paper	N/A
pcDNA3: CDK5GFP	Dr. Li-Huei Tsai (MIT)	Addgene #1346
pCMV: P35	Dr. Li-Huei Tsai (MIT)	Addgene #1347
pCEP4: 4HA-CKIε	Rivers et al., 1998	Addgene #13724
pcDNA3: GSK3β S9A-HA	Stambolic and Woodgett, 1994	Addgene #14754
pHACE: PKCα catalytic subunit-HA	Soh and Weinstein, 2003	Addgene #21234
pRC/CMV: CK2α-3HA	Turowec et al., 2010	Addgene #27086
pEGFP: HA-Akt	Watton and Downward, 1999	Addgene #39531
pCAGGS: mouse PKA catalytic subunit α-mEGFP	Zhong et al., 2009	Addgene #45528
pCIP: AMPKα1	Young et al., 2016	Addgene #79010
pcDNA3.1: human CDKL5-3xFLAG	Dr. Teruyuki Tanaka (The Univ of Tokyo)	N/A
pEGFP-C1: rat CaMKIIα	Marsden et al., 2010	N/A
pEGFP-N2: rat CaMKIIα catalytic region (aa 1-290)	This paper	N/A
pCAGGS: HA-mouse μ2-Adaptin	This paper	N/A
Software and algorithms		
PhosphoSitePlus	Cell Signaling Technology	https://www.phosphosite.org/homeAction.action
Mascot version 2.6.1	Matrix Science	http://www.matrixscience.com/mascot_support_v2_6.html
Proteome Discoverer software version 2.2	Thermo Fisher Scientific	https://www.thermofisher.com/store/products/OPTON-30945#/OPTON-30945
Leica LAS AF	Leica Microsystems	https://www.leica-microsystems.com/
Leica Application Suite X	Leica Microsystems	https://www.leica-microsystems.com/
PyMOL	Schrödinger, LLC	https://pymol.org/2/
XDS	Kabsch, 2010	https://xds.mr.mpg.de/
CCP4	Winn et al., 2011	https://www.ccp4.ac.uk/
MOLREP	Vagin and Teplyakov, 1997	http://legacy.ccp4.ac.uk/html/molrep.html
Coot	Emsley et al., 2010	https://www2.mrc-lmb.cam.ac.uk/personal/pemsley/coot/
Phenix	Liebschner et al., 2019	http://www.phenix-online.org/
Ekuseru-Tokei 2012 software	BellCurve	https://bellcurve.jp/
Other		
HDR-CX680	Sony	https://www.sony.jp/

RESOURCE AVAILABILITY

Lead contact

Further information and requests for resources and reagents should be directed to and will be fulfilled by the Lead Contact, Masaki Fukata (mfukata@nips.ac.jp).

Materials availability

All unique/stable reagents generated in this study are available from the Lead Contact upon reasonable request.

Data and code availability

- The coordinates and structure factors of 14-3-3ζ–ppADAM22 (827–857) complex have been deposited in the Protein Data Bank under the accession code of 7EXE and are publicly available as of the date of publication. Original western blot images, mass spectrometry data and microscopy images reported in this paper will be shared by the lead contact upon request.
- This paper does not report original code.
- Any additional information required to reanalyze the data reported in this paper is available from the lead contact upon request.

EXPERIMENTAL MODEL AND SUBJECT DETAILS

Mice

Mouse strains used in this study include: *Adam22*^{S832A} knock-in mouse (generated in the present study), *Adam22*^{FAH} knock-in mouse (Fukata et al., 2021), *Adam22*^{cfn} and *Adam22*^{flox} mice (Ozkaynak et al., 2010), *Lgi1* knockout mouse (Fukata et al., 2010), *Actb–iCre* mouse (Zhou et al., 2018a), *Actb–FLPe* mouse (Kono et al., 2017), *Emx1–Cre* mouse (Kassai et al., 2008), *VGAT–Cre* mouse (The Jackson Laboratory stock #016962), *PV–Cre* mouse (#008069), *SOM–Cre* mouse (#013044), *Thy1–Lgi1-FH* mouse (Fukata et al., 2010), *VGAT–Lgi1-FH* (generated in the present study), *Prox1–Lgi1-FH* (Lovero et al., 2015), *KA1–Lgi1-FH* (generated in the present study), C57BL/6N mice (Japan SLC) and B6D2F1 female mice (Japan SLC). Mice were bred and maintained under specific pathogen-free conditions in a temperature- and humidity-controlled room on a 12 hours light/12 hours dark cycle with access to food and water *ad libitum* in the animal facility of NIPS. There was no randomization of mice before analysis, and the mice used in this study were selected based purely on availability including male and female mice (except for female mice to obtain embryonic mice and obtain fertilized eggs). Genotyping was performed using PCR primers as listed in Table S2. All animal studies were reviewed and approved by the ethics committees at NINS and were performed according to the institutional guidelines concerning the care and handling of experimental animals.

Rat or mouse primary neuronal culture

Primary cultured rat hippocampal neurons were prepared from rat embryonic day 18–19 embryos, seeded onto poly-L-lysine–coated 12-mm coverslips in 24-well plates and cultured in neurobasal medium supplemented with B-27 and 2 mM glutamax and 10% fetal bovine serum. After 3-h incubation, the media was changed to neurobasal medium supplemented with 2 mM glutamax and B-27. Neurons were transfected by the Amaxa nucleofector (Lonza) before seeding. Mouse cortical neurons were prepared from mouse embryonic day 16–17 embryos and seeded onto 0.1% polyethylenimine and 50 μg/ml collagen I–coated 12-mm coverslips in 24-well plates.

Cell lines

HEK293T and COS7 cells were cultured in Dulbecco's modified Eagle's medium containing 10% fetal bovine serum. Cells were transfected using Lipofectamine plus (Thermo Fisher Scientific).

METHOD DETAILS

Cloning and plasmid constructions

The following cDNAs were cloned from mouse brain total RNA by RT-PCR using primers based on the GenBank database: mouse μ2-adaptin (GenBank: U27106), 14-3-3ζ (GenBank: D83037.1) and 14-3-3ε (GenBank: Z19599). Indicated mouse ADAM22 and 14-3-3 mutants were generated by standard PCR methods. The cytoplasmic region of human ADAM22 (759-906 aa) and mouse ADAM22 (802-904 aa) were subcloned into the pEGFP-C1 and pGEX-4T-1 vectors, respectively. The catalytic domain of rat CaMKIIα (1-290 aa) was subcloned into the pEGFP-N2 vector. All PCR products were verified by DNA sequencing.

Generation of *Adam22*^{S832A} knock-in mouse

To generate the *Adam22*^{S832A} knock-in mouse, the sgRNA target sequence of mouse *Adam22* (HM004095), 5′-CCTTGCCAGGAGTT ACTGCG-3′ (sgRNA#1), was subcloned into the pX330 (Addgene #42230) vector, which expresses Cas9 and sgRNA. For a

homology-directed repair template DNA, a 144-nucleotide custom synthesized single stranded DNA repair template (Hokkaido System Science) (5′-CATTCTTGGAGTGAAAGGATTCCAGACACAAAACATATTTCAGACATCTGTGAAAATGGGAGACCTCGAAG CAAT***GCC***TGGCAAGGTAGTGAACAGTGCTCAGAATCTAAGACCTGTATTCTGGAGACCTGTAAAATGTGTTCT-3′) was designed to span the region including a part of *Adam22* exon28 and a portion of the following intron. This template was identical to the corresponding *Adam22* locus, with the exception of a mutation of the codon encoding *Adam22* serine 832 to alanine (TCC > ***GCC***, italic) and three silent mutations (underlined) to prevent the gene editing by the same sgRNA#1. Pronuclear-stage zygotes were collected from B6D2F1 (F1 hybrid between C57BL/6 and DBA/2) female mice superovulated with eCG/hCG and mated with C57BL/6 male mice. The pX330 plasmid harboring sgRNA#1 and the above single-stranded oligodeoxynucleotide were co-injected into a pronucleus of the zygotes. To select the desired founder mice, obtained F0 pups were screened by the genomic PCR analysis and subsequent direct sequencing analyses. Then, the founder mice harboring the knock-in allele were backcrossed with C57BL/6 mice for five generations. No genomic integration of the pX330 was confirmed by genomic PCR for Cas9. Two lines from two independent founder mice were established. The reduced ADAM22 expression was shared between two lines of $Adam22^{S832A/S832A}$ mice [ADAM22 level = 35.2 ± 13.2% of wild-type mice for line #1 (n = 3, mainly used in this study) and 42.4 ± 8.2% for line #2 (n = 3)].

Generation of conditional *Adam22* knockout mice

$Adam22^{cfn/cfn}$ mice, homozygous for the conditional FRT-flanked neomycin (cfn) allele, were crossed with *Actb–FLPe* deleter mice to generate the $Adam22^{flox}$ mouse line. ADAM22 levels were comparably reduced in $Adam22^{cfn/cfn}$ and $Adam22^{flox/flox}$ mice (Figure S7A). We crossed both mouse strains with specific Cre-driver mouse lines (*Emx1–Cre* and *VGAT–Cre*, described below) and obtained similar survival rates. However, in Figure 7 we only show data obtained on the $Adam22^{cfn/cfn}$ hypomorphic background, as the experimental number was larger on this background than the $Adam22^{flox/flox}$ background (Figures S7B and S7C).

To excise the floxed allele of *Adam22*, four Cre-driver mouse lines were used: (i) *Emx1–Cre* for deletion in forebrain-specific glutamatergic neurons; (ii) *VGAT–Cre* for deletion in inhibitory neurons; (iii) *PV–Cre* for deletion in parvalbumin-positive inhibitory neurons; and (iv) *SOM–Cre* for deletion in somatostatin-positive inhibitory neurons.

Generation of transgenic mice for cell-type specific LGI1 expression

To express rat LGI1 tagged with FLAG and His_6 (LGI1-FH) in a cell-type specific manner, four transgenic mouse lines were used; (i) *Thy1–Lgi1* mouse for neuronal expression of LGI1 (Fukata et al., 2010); (ii) *VGAT–Lgi1* for expression in GABAergic inhibitory neurons; (iii) *Prox1–Lgi1* for dentate granule cell-expression (Lovero et al., 2015); and (iv) *KA1–Lgi1* for expression in the hippocampal CA3 pyramidal neurons. To generate the *VGAT–Lgi1* and *KA1–Lgi1* mouse lines, the cDNAs of *Lgi1-FH* and kanamycin-resistant gene were inserted at the locus of the start codon of a *VGAT* or a *KA1* gene in the BAC clone RP23-392P11 and RP23-353O19, respectively (Figure S8B). The linearized modified BAC DNA was microinjected into BDF1 fertilized oocytes to produce transgenic mice (PhoenixBio). To discriminate between homozygous and heterozygous transgenic mice, quantitative PCR was performed using StepOnePlus real time PCR system and Power SYBR green PCR Master Mix (Applied Biosciences).

Induction and scoring of seizures

Seizure threshold was measured in one-month old mice as described (Fukata et al., 2010; Yokoi et al., 2015). PTZ was subcutaneously injected at the dose of 35 mg/kg. Following a PTZ injection, scoring of seizures was performed for 10 min after the injection as follows: 0, no response; 1, ear and facial twitching; 2, myoclonic body jerks; 3, clonic forelimb convulsions; 4, generalized clonic convulsions, turn over into side position; 5, generalized tonic convulsions. Investigators were blinded to the mouse genotypes and drug treatment for PTZ seizure test.

Biochemical analysis of brain lysates

Brains from littermate mice (P16–18) were homogenized in 5 volumes of buffer A [10 mM HEPES-Na (pH 7.5), 0.32 M sucrose and 200 μg/ml phenylmethylsulfonyl fluoride (PMSF)]. The homogenate was centrifuged at 1,000 g for 10 min at 4°C. The pellet was re-homogenized in 1 volume of buffer A and centrifuged at 1,000 g for 10 min. The first and second supernatants were mixed and centrifuged at 20,000 g for 1 h at 4°C. The pellet (P2) was solubilized with 5 volumes of buffer B [20 mM Tris-HCl (pH 8.0), 1.3% Triton X-100, 100 mM NaCl and 50 μg/ml PMSF] for 1 h at 4°C. The resuspended P2 fraction was centrifuged at 100,000 g for 1 h to produce supernatant (Triton X-100-sol) and pellet (Triton X-100-insol) fractions. Protein concentration was determined by BCA protein assay (Thermo Fisher Scientific). For comparison of protein levels, equal amounts of protein (18 μg of homogenates) were subjected to quantitative western blotting.

Endo H and PNGase F treatment

Mouse brain homogenates (40 μg of the total proteins) were denatured in a denaturing buffer (0.05% SDS, 0.1% mercaptoethanol) for 10 min at 100°C. The denatured proteins were digested with Endo H or PNGase F for 1 h at 37°C. Proteins were separated by SDS-PAGE and subjected to western blotting.

Phos-tag SDS-PAGE

Phos-tag SDS-PAGE was performed as previously reported (Kinoshita et al., 2009). Briefly, 6 or 7% acrylamide gels containing 25 mM Phos-tag acrylamide (AAL-107, Wako) and 50 mM $MnCl_2$ or 11% acrylamide gels containing 25 mM Phos-tag acrylamide

and 50 mM $Zn(NO_3)_2$ were used. After electrophoresis, the gel was washed with blotting buffer containing 1 mM EDTA for 10 min, and proteins were transferred to the PVDF membrane for western blotting. For Figure 1D, to detect the exogenously expressed mouse ADAM22 mutants, the anti-ADAM22 antibody (R2) which reacts with predominantly mouse ADAM22 over rat ADAM22 was used for western blotting.

Immunoprecipitation from the mouse brain

Forebrains from littermate mice (P17–18) were homogenized in buffer C [20 mM Tris-HCl (pH 8.0), 0.32 M sucrose, 2 mM EDTA, 5 mM sodium fluoride and 50 μg/ml PMSF]. After centrifugation at 20,000 g for 1 h at 4°C, the pellet was solubilized with buffer D [20 mM Tris-HCl (pH 8.0), 1.3% Triton X-100, 100 mM NaCl, 1 mM EDTA, 5 mM sodium fluoride, 2 mM sodium pyrophosphate and 50 μg/ml PMSF] for 1 h at 4°C. After centrifugation at 100,000 g for 1 h at 4°C, the supernatant was precleared and incubated with 5 μg of anti-ADAM22 antibodies overnight at 4°C. The immunecomplexes were then precipitated with Protein A Sepharose. The purified immunecomplexes were separated by SDS-PAGE, followed by western blotting or silver staining. The specific protein bands coimmunoprecipitated with ADAM22 were excised from a silver-stained gel and analyzed with mass spectrometry as described (Fukata et al., 2021).

Reprecipitation of PSD-95 from ADAM22-containing complexes

Whole brains from wild-type or *Adam22*$^{FAH/FAH}$ mice (P70–75) were homogenized in buffer C. After centrifugation at 20,000 g for 1 h at 4°C, the pellet was solubilized with buffer D for 1 h at 4°C. After centrifugation at 100,000 g for 1 h at 4°C, the supernatant was precleared and incubated with anti-FLAG-M2 affinity gel overnight at 4°C. The first eluate was obtained with 20 mM Tris-HCl (pH 7.5) buffer containing 0.1% Triton X-100, 100 mM NaCl, 5 mM sodium fluoride, 2 mM sodium pyrophosphate, 50 μg/ml PMSF and 0.25 mg/ml FLAG peptide. For reprecipitation of PSD-95, the eluate was incubated with 5 μg of anti-PSD-95 antibody (Noritake et al., 2009) for 1 h at 4°C. The immunecomplexes were then precipitated with Protein A Sepharose. The purified immunecomplexes were separated by SDS-PAGE, followed by western blotting.

Determination of ADAM22 phosphorylation sites

ADAM22 protein was immunoprecipitated from *Adam22*$^{+/+}$, *Adam22*$^{SA/SA}$ or *Adam22*$^{FAH/FAH}$ (Fukata et al., 2021) mouse brains. The immunoprecipitates were separated by SDS-PAGE and subjected to silver staining. The protein bands corresponding to ADAM22 were excised, digested using trypsin, and analyzed on an Orbitrap Elite mass spectrometer (Thermo Fisher Scientific) as described (Fukata et al., 2021). The MS/MS data were acquired by collision-induced dissociation (CID) or higher energy collisional dissociation fragmentation. The database search was performed using the MASCOT (ver. 2.6.1, Matrix science, London) with the following parameters: enzyme (trypsin allowed up to 2 missed cleavages); fixed modifications (carbamidomethyl at cysteine residue); variable modifications (oxidation at methionine residue, phosphorylation at serine and threonine residues, phosphorylation at tyrosine residue, and diglycine at lysine residue); peptide mass tolerance for precursor ions (±10 ppm); and mass tolerance for fragment ions (±0.8 kDa). The MS/MS spectra of all phosphopeptides detected in the database search were manually checked to determine the phosphorylation residues (by a loss of mass of 98 Da, as a signature for the CID-induced fragment ion containing the phosphoserine/threonine residue). The number of phosphopeptides detected from four independent analyses were summarized in Figure 1B. MS analysis was performed in Functional Genomics Facility, National institute for basic biology (NIBB) Core Research Facilities.

In vitro phosphorylation assay

Bacterially expressed GST-fused cytoplasmic region of ADAM22 (~700 ng) was purified and incubated with the PKA catalytic subunit (30 Unit) in 60 μL kinase assay buffer [50 mM Tris-HCl (pH 7.5), 10 mM $MgCl_2$, and 0.2 mM ATP] for 30 min at 30°C. Phosphorylation of ADAM22 was examined by Phos-Tag SDS-PAGE and western blotting with ADAM22-S832 phospho-specific antibody. To further determine the phosphorylation sites of ADAM22, the ADAM22 band was excised, subjected to MS analysis as above.

Blue-Native PAGE

Forebrains including hippocampus and cortex were homogenized in 20 volumes buffer E [1 mM HEPES-Na (pH 7.4), 0.32 M sucrose and 200 μg/ml PMSF]. The homogenates were centrifuged at 1,000 g for 10 min at 4°C and the supernatants were followed by an additional 10 min spin at 1,000 g. After centrifugation of the supernatants at 20,000 g for 1 h, pellets were solubilized for 1 h in 20 volumes of buffer F [25 mM Tris-HCl (pH 8.0), 1% Triton X-100 and 500 mM aminocaproic acid]. After centrifugation at 20,000 g for 20 min, solubilized protein was mixed in a 10:1 ratio with the loading solution (50% glycerol and 0.1% ponceau S). Native acrylamide gradient gels (1.5%–13%) and cathode/anode buffers were prepared as described previously (Schägger, 2001; Wittig et al., 2006). After electrophoresis, gels were washed at room temperature with NuPAGE transfer buffer (Invitrogen), and proteins were transferred onto PVDF membranes. The membranes were incubated with 8% acetic acid for 15 min to fix proteins, and destained for 15 min in 10% acetic acid/25% methanol for western blot analysis.

Purification from heterologous cells

For immunoaffinity purification in Figure 4F, FLAG-tagged ADAM22 and HA-tagged μ2-adaptin were co-transfected into COS7 cells. The cells were washed with PBS and incubated in buffer G [20 mM Tris-HCl (pH 7.5), 1.0% Triton X-100, 150 mM NaCl, 1 mM EDTA,

5 mM sodium fluoride, 5 mM sodium pyrophosphate and 50 μg/ml PMSF] for 30 min at 4°C. After centrifugation at 20,000 g for 30 min, the supernatant was incubated with anti-FLAG M2 agarose. The elution was achieved by the addition of buffer G containing 0.25 mg/ml FLAG peptide. For Figure 4G, ADAM22 and His_6-tagged 14-3-3 were cotransfected into HEK293T cells. After 45-h serum starvation, the cells were incubated with 50 μM forskolin for 15 h. His_6-tagged 14-3-3 was pulled down with TALON Metal Affinity Resin (Clontech).

Cell-surface biotinylation assay

Transfected COS7 cells were washed with ice-cold buffer H (PBS with 1 mM $MgCl_2$ and 0.1 mM $CaCl_2$) three times at 4°C, and incubated with 2.3 mM Sulfo-NHS-Biotin (Thermo Fisher Scientific) for 30 min at 4°C. Then, cells were washed with ice-cold buffer H, incubated with buffer H containing 100 mM glycine for 5 min and washed with ice-cold buffer H twice at 4°C. The cells were lysed in buffer I [20 mM Tris-HCl (pH 7.5), 1 mM EDTA, 100 mM NaCl, 1% SDS, and 50 μg/ml PMSF]. After a 20 min extraction, the lysates were diluted with 10 volumes of buffer I containing 1% Triton X-100 instead of SDS. After centrifugation at 20,000 g for 30 min, the supernatant was incubated with Pierce High Capacity NeutrAvidin agarose beads (Thermo Fisher Scientific) for 12 h at 4°C and eluted with SDS sample buffer.

Quantitative western blotting

Chemical luminescent signal was detected with FUSION Solo (Vilber-Lourmat). The band intensities were analyzed with the FUSION Capt software or CS analyzer 3.0 software (ATTO).

Immunohistochemistry

Mice were treated by pentobarbital (100 mg/kg, i.p.) and perfused with 4% paraformaldehyde in 0.1 M phosphate buffer (pH 7.4). The brain was removed and immersed in the same fixative overnight at 4°C and then cryoprotected in 20% sucrose in PBS overnight at 4°C. The 60-μm free-floating sections were cut on a cryostat (CM1950; Leica). For antigen-exposing pretreatment, sections were incubated with 0.2 mg/ml pepsin (DAKO) for 10 min at 37°C. Sections were blocked in PBS containing 3% normal goat serum and 0.1% Triton X-100 for 1 h at room temperature and then incubated in the same buffer containing ADAM22 or LGI1 antibodies for 40 h at 4°C. Endogenous peroxidase activity was inactivated by incubating brain sections in PBS containing 1% H_2O_2 for 15 min. Sections were treated with avidin-biotin complex (ABC Elite, Vector Laboratories) for 1 h and incubated with DAB substrate for 2-3 min until development of optimum brown color (the same incubation time used for comparison). Images were taken using stereomicroscope equipped with a digital camera (Olympus DP20) with the same exposure time and camera setting.

For immunohistofluorescence staining, freshly dissected brains were frozen in *n*-hexane cooled on dry ice and embedded in OCT compound. Then, the frozen sections (7 μm in thickness) were cut on a cryostat (CM1950, Leica) and fixed with acetone for 20 min on ice (on glass slides). The sections were rehydrated and blocked in PBS containing 10% normal donkey serum for 1 h at room temperature and were incubated with an anti-FH antibody for 2 h at room temperature, followed by Alexa488-conjugated secondary antibodies. Fluorescent images were acquired with a confocal laser scanning microscopy system (TCS SP5II; Leica) equipped with an HC PL APO 20 × /0.70 objective lens. Microscope control and all image analyses were performed with Leica LAS AF software, and images were acquired with the same laser power and detector settings for comparison.

Immunofluorescence analysis of cultured neurons

Cultured mouse cortical neurons (4×10^4 cells) were seeded onto 12-mm coverslips in 24-well plates. Neurons were fixed with 4% paraformaldehyde/120 mM sucrose/100 mM HEPES-Na (pH 7.4) at room temperature for 10 min and permeabilized with 0.1% Triton X-100 for 10 min on ice, or fixed with methanol for 10 min at –30°C. Then, neurons were blocked with PBS containing 10 mg/ml BSA for 10 min on ice, and incubated with indicated antibodies for 1 h at room temperature, followed by Alexa488-, Cy3-, and Alexa647-conjugated secondary antibodies. Fluorescent images were acquired with a confocal laser scanning microscopy system (TCS SP5II; Leica) equipped with an HCX PL APO 63 × /1.40-0.60 oil immersion objective lens. Microscope control and all image analyses were performed with Leica LAS AF software, and images were acquired with the same laser power and detector settings for comparison.

ITC

The ITC measurements were performed using MicroCal Auto-iTC200 (Malvern Panalytical). The cell contained 50 μM 14-3-3ε and the syringe contained 1.0 mM singly-phosphorylated pADAM22 peptide or 0.5 mM doubly-phosphorylated ppADAM22 peptide in buffer J [20 mM HEPES-Na (pH 7.5), 150 mM NaCl]. A series of 2 μL titrations were performed at 25°C. Dissociation constants (K_d) were calculated by fitting the data with a one-site binding model using the software Origin (MicroCal). pADAM22 peptide (^{827}RPRSN**pS**WQGN^{836}) and ppADAM22 peptide (^{827}RPRSN**pS**WQGNMGGNKKKIRGKRFRPRSN**pS**TE^{857}) were synthesized by Eurofins Genomics and SCRUM Inc., respectively.

Crystallography of 14-3-3ζ–ppADAM22 complex

Mouse 14-3-3ζ (GenBank: D83037.1) containing an N-terminal His_6 tag was expressed in *Escherichia coli* Rosetta (DE3) cells (Merck Millipore). The cells were cultured in LB medium containing 100 mg/l ampicillin at 37°C until the optical density at 600 nm of the culture reached 0.5–0.8. The expression was induced by adding 0.1 mM isopropyl-β-D-1-thiogalactopyranoside to the culture. The cells

were further cultured for 12 h at 15°C and then harvested by centrifugation. The harvested cells were suspended in 50 mM Tris-HCl buffer (pH 8.0) containing 150 mM NaCl, 20 mM imidazole, and 0.5% Triton X-100, and disrupted by sonication. The lysate was cleared by centrifugation at 37,600 g for 1 h at 4°C. The His_6-tagged 14-3-3ζ was purified using Ni-nitrilotriacetic acid agarose (QIAGEN) according to the manufacturer's manual. After washing with 50 mM Tris-HCl buffer (pH 8.0) containing 150 mM NaCl and 20 mM imidazole, the protein was eluted with 50 mM Tris-HCl buffer (pH 8.0) containing 150 mM NaCl and 200 mM imidazole. The eluted protein was further purified by size-exclusion chromatography using a HiLoad 16/600 Superdex 75 pg (Cytiva) column with 20 mM HEPES-Na buffer (pH 7.5) containing 150 mM NaCl. The fractions abundant in the protein were collected and concentrated to 11.5 g/l using an Amicon Ultra-15 Centrifugal Filters (MWCO 10,000; Merck Millipore). The protein was aliquoted, flash-frozen in liquid N_2, and stored at –80°C.

Initial crystallization screening was performed using the sitting drop vapor diffusion method at 20°C with a Mosquito liquid-handling robot (TTP Lab Tech). About 1,000 conditions were tested with crystallization reagent kits supplied by Hampton Research and Molecular Dimensions. 14-3-3ζ (10.5 g/l) was mixed with ppADAM22 in a molar ratio of 1.4:1:2 (14-3-3ζ dimer:peptide:fusicoccin-A) and incubated on ice for 6 h before crystallization setup. The best crystal was obtained with the reservoir solution containing 0.2 M trimethylamine *N*-oxide dihydrate, 0.1 M Tris-HCl (pH 8.5), 20% (w/v) polyethylene glycol monomethyl ether 2,000, 10 mM $BaCl_2$ dihydrate, and 4% (v/v) pentaerythritol ethoxylate (3/4 EO/OH). The crystal was soaked in the reservoir solution supplemented with 28% ethylene glycol, and then flash-frozen in liquid N_2.

Diffraction datasets were collected at 100 K at BL45XU in SPring-8 and processed with XDS (Kabsch, 2010) and the CCP4 program suite (Winn et al., 2011). The 14-3-3ζ structure was determined by molecular replacement with the program MOLREP (Vagin and Teplyakov, 1997) using the structure of human 14-3-3ζ in complex with a phosphopeptide (PDB: 1QJA) as the search model. The atomic model of ppADAM22 was manually built using the program Coot (Emsley et al., 2010). No electron density corresponding to fusicoccin-A was found. The ppADAM22–14-3-3ζ structure was refined using the program Phenix (Liebschner et al., 2019). Iterative model building and refinement improved the model with good stereochemistry (97.3% and 0.00% of residues in Ramachandran favored and outliers, respectively). Data collection and refinement statistics are summarized in Table S1. All structure figures were prepared using the program PyMOL (Schrödinger, LLC; https://pymol.org/2/).

QUANTIFICATION AND STATISTICAL ANALYSIS

To perform statistical analysis, at least 3 experiments were performed for independent tissue samples or mice, as described in figure legends, except for Figure 4G. We excluded mice if we observed any abnormality in terms of size and weight in mice before performing experiments. The mice in this study were not randomized to their treatments and were selected based purely on availability. For Figures 6B and 6C, investigators were blinded. No statistical method was used to determine sample size, and sample sizes are consistent with those reported in similar studies. No significant differences in variance between groups were detected using an F test. For comparisons of two groups, two-tailed Student's t test was used (Figures 2G and 3A). For multiple test subjects, one-way ANOVA followed by post hoc Tukey's test (Figures 2B, 3B, 3E, 4C, 4F, S4, and S7A) and Dunnett's test (Figures 6F and S6) were used. If the equal variance test failed, we performed one-tailed, one-sample Student's t test (Figure 4G) and Kruskal-Wallis one-way ANOVA followed by post hoc Steel's test (Figures 4G and 6B). Survival curves of mutant mice were analyzed by Kaplan-Meier survival estimate using a log-rank test for curve comparisons (Figure 7D). Statistical analysis was performed with Ekuseru-Toukei 2012 software (SSRI). Results are shown as means ± SD. Statistical significance was defined as $*p < 0.05$; $**p < 0.01$; $***p < 0.001$.